

1 **THE MEAN VOLUME AS A LOCAL QUALITY MEASURE**
 2 **FOR EFFICIENT MESH OPTIMIZATION**

3 DIMITRIS VARTZIOTIS^{†‡§} AND BENJAMIN HIMPEL[†]

4 **Abstract.** The signed volume function for polyhedra can be generalized to a mean volume function for
 5 volume elements by averaging over the triangulations of the underlying polyhedron. If we consider these up to
 6 translation and scaling, the resulting quotient space is diffeomorphic to a sphere. The mean volume function
 7 restricted to this sphere is a quality measure for volume elements. We show that, the gradient ascent of this
 8 map regularizes the building blocks of hybrid meshes consisting of tetrahedra, hexahedra, prisms, pyramids and
 9 octahedra, that is, the optimization process converges to regular polyhedra. We show that the (normalized)
 10 gradient flow of the mean volume yields a fast and efficient optimization scheme for the finite element method
 11 known as the geometric element transformation method (GETMe). Furthermore, we shed some light on the
 12 dynamics of this method and the resulting smoothing procedure both theoretically and experimentally.

13 **Key words.** hybrid mesh, smoothing, quality metric, quality measure, polyhedron, optimization, finite
 14 element method, GETMe, octahedron, tetrahedron, hexahedron, pyramid, prism

15 **AMS subject classifications.** 52B70, 58C05, 37C10

16 **1. Introduction.** In the context of the finite element method, mesh quality affects nu-
 17 merical stability as well as solution accuracy of this method [38]. The geometric element trans-
 18 formation method (GETMe) as a smoothing and untangling algorithm for tetrahedral meshes
 19 is introduced in [46], which was generalized to hybrid meshes in [41, 42, 43, 44, 45]. We consider
 20 GETMe as a class of smoothing methods based on simple geometric transformations applied it-
 21 eratively to all elements individually. Several numerical tests have confirmed that the geometric
 22 element transformation given in [46] and its generalizations reliably and efficiently regularizes
 23 the polyhedron types, which are relevant for the finite element method. In this paper, regu-
 24 larization refers to the convergence of the iteratively transformed polyhedra towards a regular
 25 polyhedron, and we ask the reader not to confuse this terminology with the methods in nu-
 26 merical analysis that allow you to deal with ill-conditioned problems. GETMe smoothing also
 27 significantly reduces errors in solutions of the finite element method and improves solution ef-
 28 ficiency for meshes [45]. The search for a mathematical proof of its qualitative behavior led us
 29 to the discovery of a simple and reasonable quality measure for volume elements optimized by
 30 polyhedral generalizations of the tetrahedral GETMe algorithm in [46]. Therefore, the purpose
 31 of our work is threefold:

- 32 1. We introduce the mean volume and turn it into a scaling-invariant quality measure.
- 33 2. We consider the gradient flow of the mean volume and discuss its close relationship to the
 34 tetrahedral GETMe algorithm presented in [46].
- 35 3. We analyze the new GETMe optimizing and untangling algorithms for volume elements
 36 induced by the gradient flow of the mean volume both theoretically and experimentally.

37 Mesh smoothing methods can be classified [29, 31, 47] as geometry-based [16, 46], optimi-
 38 zation-based [14, 7, 18, 20, 32, 37, 26, 35, 8], physics-based [36] and combinations thereof
 39 [9, 17, 10]. In order to be more effective, these methods need to be combined with topological
 40 modifications [5, 19, 22]. Local or global Optimization-based methods effectively optimize an
 41 objective function measuring the quality of elements or the mesh as a whole. They often

[†]TWT GmbH Science & Innovation, Department for Mathematical Research & Services, Bernhäuser
 Straße 40–42, 73765 Neuhausen, Germany

[‡]NIKI Ltd. Digital Engineering, Research Center, 205 Ethnikis Antistasis Street, 45500 Katsika, Ioannina,
 Greece

[§]Corresponding author. E-mail address: dimitris.vartziotis@nikitec.gr

lend themselves to untangling algorithms [24, 27, 20, 2, 14]. Geometry-based methods like the Laplacian [16] and GETMe [46] smoothings have the advantage of being exceptionally fast, but their effect on the quality of a mesh is heuristic. Therefore it came as a surprise, that a minor variation of the GETMe method presented in [46] generalizes to a local optimization-based mesh smoothing and untangling method for hybrid meshes with an objective function induced by a generalization of the volume function.

After a review of the GETMe algorithm [46] in §2 we introduce the mean volume in §3. Section 4 establishes the intimate relationship of the mean volume and the GETMe algorithm by way of the gradient field. We leverage this relationship in §5 in order to give a natural generalization of the GETMe smoothing procedure to other volume elements and hybrid meshes. Before we discuss the dynamics of these optimization and smoothing methods both from a theoretical and experimental point of view in §7, it is instructive to rigorously show that certain singularities of the gradient of the mean volume correspond to regular polyhedra in §6. We finish with a summary in §8 and an outlook to global optimization-based GETMe methods.

2. The tetrahedral GETMe algorithm. In [46] a heuristic method for smoothing tetrahedral meshes was developed and further generalized to other volume elements in [41, 42, 43, 44, 45]. Let us review the key algorithm and results from [46].

2.1. Transformation of a tetrahedron. Let $\tau = (x_1, x_2, x_3, x_4)^t \in \mathbb{R}^{12}$ denote a tetrahedron with the four pairwise disjoint nodes $x_i \in \mathbb{R}^3$, $i \in \{1, \dots, 4\}$, which is positively oriented. That is, $\det(D(\tau)) > 0$ with

$$(2.1) \quad D(\tau) := (x_2 - x_1, x_3 - x_1, x_4 - x_1)$$

representing the (3×3) -matrix of the difference vectors, which span the tetrahedron τ . Furthermore, let

$$(2.2) \quad \begin{aligned} n_1 &:= (x_4 - x_2) \times (x_3 - x_2) \\ n_2 &:= (x_4 - x_3) \times (x_1 - x_3) \\ n_3 &:= (x_2 - x_4) \times (x_1 - x_4) \\ n_4 &:= (x_2 - x_1) \times (x_3 - x_1). \end{aligned}$$

denote the inside oriented face normals of τ .

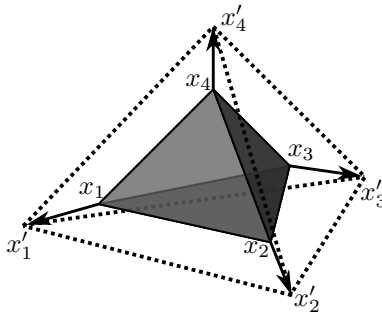


Fig. 2.1: Transformation of a tetrahedron

A new tetrahedron τ' with nodes x'_i is derived from τ by translating each node x_i using the

66 opposing face normal n_i scaled by $\sigma/\sqrt{|n_i|}$ for some fixed $\sigma \in \mathbb{R}_0^+$. That is,

$$(2.3) \quad \tau' = \begin{pmatrix} x'_1 \\ x'_2 \\ x'_3 \\ x'_4 \end{pmatrix} := \begin{pmatrix} x_1 \\ x_2 \\ x_3 \\ x_4 \end{pmatrix} + \sigma \begin{pmatrix} \frac{1}{\sqrt{|n_1|}} n_1 \\ \frac{1}{\sqrt{|n_2|}} n_2 \\ \frac{1}{\sqrt{|n_3|}} n_3 \\ \frac{1}{\sqrt{|n_4|}} n_4 \end{pmatrix}.$$

67 An initial tetrahedron τ and its transformed counterpart τ' are depicted in Figure 2.1. The
68 edges of the resulting tetrahedron τ' are indicated by dotted lines.

69 **2.2. Properties of the transformation.** The quality of tetrahedra is measured by the
70 mean ratio function [23]

$$(2.4) \quad q(\tau) := \frac{3 \det(S)^{2/3}}{\|S\|_F^2}$$

71 with $\|S\|_F := \sqrt{\text{tr}(S^t S)}$ denoting the Frobenius norm of the matrix $S := DW^{-1}$. Here D
72 represents the difference matrix given in (2.1), and W denotes the difference matrix of a regular
73 tetrahedron. It holds that $q(\tau) \in [0, 1]$, where very small values indicate nearly degenerate
74 tetrahedra and larger values almost regular tetrahedra. In particular it holds that $q(\tau) = 1$,
75 if τ is regular. It has been tested heuristically that GETMe increases the mean ratio quality
76 function in (2.4), and that σ controls the speed in analogy to the results in Figure 7.2.

77 **2.3. GETMe smoothing of tetrahedral meshes.** A tetrahedral mesh consists of $n \in \mathbb{N}$
78 nodes $x_i \in \mathbb{R}^3$ and $m \in \mathbb{N}$ tetrahedra $\tau_j = (x_{i_{j,1}}, x_{i_{j,2}}, x_{i_{j,3}}, x_{i_{j,4}})^t$, where $i_{j,k} \in \{1, \dots, n\}$,
79 $j = 1, \dots, m$ and $k = 1, \dots, 4$. Indices of the nodes for each tetrahedron are ordered such that
80 all tetrahedra τ_j are valid in the sense that they are positively oriented.

81 Measures for the quality of a tetrahedral mesh are the minimal mean ratio number

$$(2.5) \quad q_{\min} := \min_{j \in \{1, \dots, m\}} q(\tau_j)$$

82 and the mean value of all mean ratio numbers

$$(2.6) \quad q_{\text{mean}} := \frac{1}{m} \sum_{j=1}^m q(\tau_j).$$

83 GETMe smoothing algorithms based on Equation (2.3) combine the transformation with a
84 simple scaling and relaxation procedure in order to improve the overall mean ratio mesh quality,
85 while preserving the validity of all tetrahedra after every iteration step. Scaling is an important
86 aspect of the smoothing procedure, which will leave one of the properties volume, surface area
87 and edge length sum unchanged. There are two flavors:

- 88 • The simultaneous smoothing applies the transformation simultaneously to all tetrahedra.
 - 89 • The sequential smoothing applies the transformation iteratively to the worst tetrahedron.
- 90 Usually, the simultaneous and sequential methods have been combined by first simultaneously
91 smoothing the mesh, and then optimizing particularly bad elements by sequential smoothing.

92 **2.4. Results.** GETMe, Smart Laplace and Mesquite Global Optimization smoothing algo-
93 rithms have been compared with regard to speed and mean ratio quality for several academic
94 and industrial examples. See Figure 2.2 and Figure 2.3 in the case of a ball triangulated by
95 tetrahedra. Since Mesquite by its very implementation optimizes the overall mean ratio quality

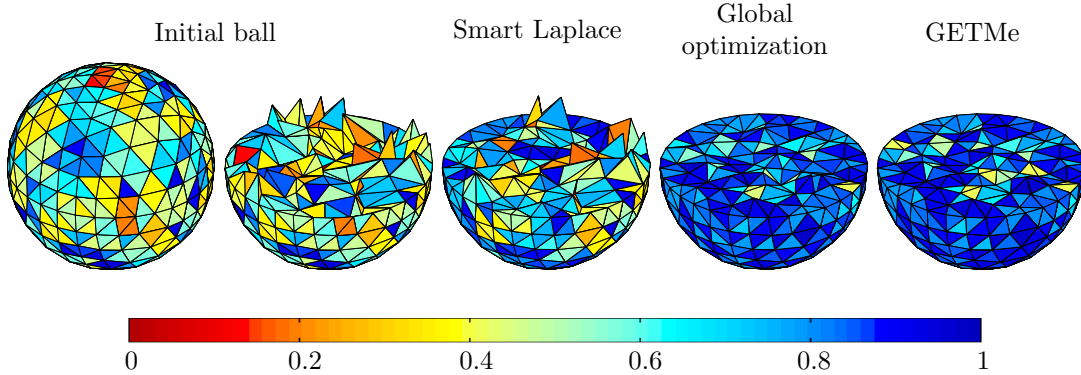


Fig. 2.2: Initial triangulated ball, its lower hemisphere, and smoothed meshes, with elements colored according to their mean ratio quality number.

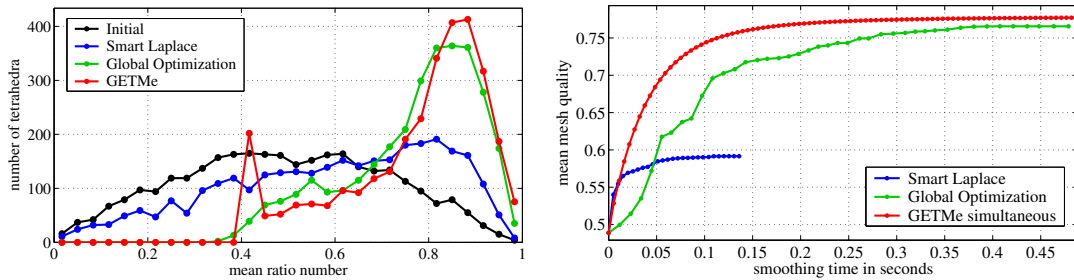


Fig. 2.3: Mesh quality histogram and mesh quality improvement with respect to smoothing time.

96 using the Newton method, it is astonishing, that the GETMe algorithm not only reaches the
 97 same quality, but is more efficient. Similarly impressive results have been achieved for the 12
 98 sample meshes from [22, 1].

99 *Remark 2.1.* In the case of inverted elements the mesh has to be untangled in a preprocessing
 100 step as described, for example, in [20]. Even though GETMe smoothing itself is suitable for
 101 untangling the mesh, this has not been analyzed in detail.

102 **3. The mean volume for volume elements.** At first sight, the volume of a polyhedron
 103 seems like a rather useless quality measure for polyhedra, because it lacks scaling-invariance
 104 and cannot capture information about the (scaling-invariant) shape of the object. It is therefore
 105 interesting, that there should be a simple way to turn it into a useful element quality measure
 106 for hybrid meshes. First of all, we need to extend the volume to a more abstract notion of
 107 volume elements, the building blocks of hybrid meshes. These volume elements are essentially
 108 polyhedra, for which we allow non-planar faces and self-intersections. We call this generalization
 109 mean volume, and it is defined via triangulations of the underlying polyhedra. This step is
 110 followed by a suitable normalization procedure in order to get a scaling-invariant quality measure
 111 from the volume.

112 **3.1. Triangulations.** Every convex polyhedron can be triangulated. For example, a pyra-
 113 mid $P = (x_1, \dots, x_5)$ with apex x_5 allows for the two different triangulations depicted in Fig-

ure 3.1.

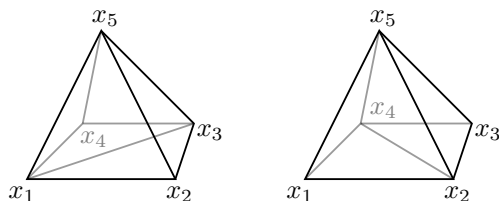


Fig. 3.1: The different triangulations of a pyramid

114

115 DEFINITION 3.1. A triangulation of a convex polyhedron P is given by a family $T =$
 116 $\{\tau_i\}_{i=1,\dots,m}$, $m \in \mathbb{N}$, of positively oriented tetrahedra τ_i , such that

- 117 1. $P = \bigcup_i \tau_i$, and
 118 2. $\tau_i \cap \tau_j$ is either the empty set, a node or a facet for $i \neq j$.

119 Observe, that the number m of tetrahedra can be different for different triangulations of
 120 the same polyhedron. For example, there are triangulations of a hexahedron with 5 and with 6
 121 tetrahedra.

122 Volume elements are always associated to some underlying reference polyhedron. This
 123 allows us to triangulate any volume element by using the triangulations of the underlying
 124 polyhedron. If x_1, \dots, x_k are the nodes of the volume element, it will be convenient to denote
 125 the volume element itself by $x = (x_1, \dots, x_k)^t \in \mathbb{R}^{3k}$, especially since we will treat x as point
 126 on a manifold. For tetrahedra, the formal distinction between τ and x is supposed to clarify,
 127 whether the tetrahedron is considered as a volume element or as a polyhedron. While this might
 128 seem unnecessary for tetrahedra, it is helpful in the discussion of other volume elements and
 129 polyhedra. For example, we have two triangulations of the volume element $x = (x_1, \dots, x_5)^t$
 130 shown in Figure 3.2, where the reference polyhedron is the pyramid shown with its triangulations
 131 in Figure 3.1. Notice, that only the third tetrahedron in Figure 3.2 is positively oriented, the
 132 others are negatively oriented. In particular, there is no canonical three-dimensional geometric
 object corresponding to this volume element.

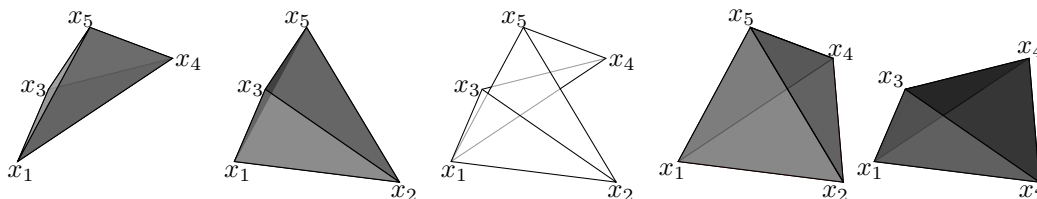


Fig. 3.2: A volume element based on the pyramid and its two triangulations (left and right) consisting of two tetrahedra each

133

134 Given a volume element x , let us denote by \mathcal{T}_x the set of all triangulations of x corresponding
 135 to the triangulations of its underlying polyhedron as described in Definition 3.1.

136 **3.2. The mean volume.** The signed volume of a tetrahedron with vertex coordinates
 137 $\tau = (x_1, \dots, x_4) \in \mathbb{R}^{3 \times 4}$ agrees with $1/6$ of the determinant of the difference matrix (2.1) and
 138 can also be written as

$$(3.1) \quad \text{vol}(\tau) = \frac{1}{6}((x_2 - x_1) \times (x_3 - x_1)) \cdot (x_4 - x_1).$$

139 The orientation of the tetrahedron and therefore the sign of the volume function is determined
 140 by the order of vertices. Notice, that it is therefore not only a well-defined function for valid
 141 tetrahedra, but also for invalid and degenerate tetrahedra.

142 We also have a signed volume function for polyhedra. Given a convex polyhedron P , we
 143 may consider a triangulation T of P and compute

$$(3.2) \quad \text{vol}(P) = \sum_{\tau \in T} \text{vol}(\tau).$$

144 We can also compute this volume function for a volume element. Since the facets are not
 145 necessarily planar, this function depends on the triangulation T . Given a volume element x , we
 146 can however simply take the average over all triangulation \mathcal{T}_x .

147 **DEFINITION 3.2.** *The mean volume of a volume element x is given by*

$$\text{vol}(x) = \frac{1}{|\mathcal{T}_x|} \sum_{T \in \mathcal{T}_x} \sum_{\tau \in T} \text{vol}(\tau).$$

148 There are alternative definitions for this mean volume function, but this is the most convenient
 149 one for our purpose. Notice that there are non-planar polyhedra, for which the mean volume
 150 vanishes. For example, the volume element in Figure 3.2 is such an example: only the volume
 151 of the third polyhedron is positive, the other three smaller tetrahedra have negative volume.

152 The mean volume for volume elements generalizes the (generalized) volume for triangu-
 153 lated polyhedral surfaces introduced by Connelly [11], which was used in the proof of the
 154 bellows conjecture [12, 34]. The quadrilateral (non-planar) facets of the volume elements can
 155 be geometrically realized by certain doubly-ruled surfaces [13]. In applications, we usually only
 156 encounter meshes with triangular and quadrilateral facets, and the use of the doubly-ruled sur-
 157 faces allows us to treat the volume elements as 3-dimensional objects whose volume equals the
 158 mean volume.

159 **3.3. The quality measure.** Clearly, the mean volume function is translation-invariant,
 160 but not scaling-invariant. However, there are several ways to make it scaling-invariant by
 161 normalizing it. There is the Frobenius norm used in the mean ratio function (2.4), or we
 162 could use a combination of edge length and area. Instead we define for a volume element
 163 $x = (x_1, \dots, x_k)^t$, for which not all coordinates are equal,

$$(3.3) \quad \begin{aligned} \pi: \quad \mathbb{R}^{3k} &\rightarrow \mathbb{R}^{3k} \\ (x_1, \dots, x_k)^t &\mapsto \frac{(x_1 - x_*, \dots, x_k - x_*)^t}{\|(x_1 - x_*, \dots, x_k - x_*)^t\|}, \quad \text{where } x_* = \sum_{i=1}^k x_i. \end{aligned}$$

164 The function π translates a volume element to its centroid and rescales it. Since e is not
 165 entirely degenerate, $(x_1 - x_*, \dots, x_k - x_*)$ does not vanish and π is well-defined. The function
 166 $q: \mathbb{R}^{3k} \rightarrow \mathbb{R}$ given by

$$(3.4) \quad q = \text{vol} \circ \pi$$

167 is invariant under scaling, translation and rotation, and we will consider it as quality measure
 168 for volume elements.

169 As we will see, regular tetrahedra, hexahedra, octahedra as well as certain symmetric pyra-
 170 mids and prisms maximize this function. Numerical tests and some theoretical evidence suggest,
 171 that the global maximum is the only local maximum for all of these volume elements. In par-
 172 ticular, optimizing a hybrid mesh with respect to this quality measure should generally improve
 173 meshes for its use in finite-element analysis.

174 **4. The gradient of the mean volume.** Following the gradient flow lines of the mean
 175 volume quality measure will certainly improve the volume elements with respect to this quality
 176 measure. In this section we will see how the mean volume from §3 relates to the tetrahedral
 177 GETMe algorithm described in §2. We find it instructive to introduce a mathematical model
 178 for the space of volume elements with a fixed underlying polyhedron, which incorporates the
 179 desired invariance under scaling and translation of quality functions.

180 **4.1. The manifold of volume elements.** Quality measures are often invariant under
 181 scaling, translation and rotation. Therefore, we want to find a model for the space of volume
 182 elements, on which the analysis of such quality measures is simplified. If we leave out rotations,
 183 we will see that the resulting model is simply a sphere.

184 The space of volume elements $x = (x_1, \dots, x_k)^t$ is isomorphic to the Euclidean space \mathbb{R}^{3k} .
 185 Considering these elements up to translation and scaling corresponds to introducing an equiv-
 186 alence relation on \mathbb{R}^{3k} defined by

$$x \sim x' :\iff x = \lambda x' + (x_0, \dots, x_0)^t \text{ for some } \lambda' \in \mathbb{R} \setminus \{0\} \text{ and } x_0 \in \mathbb{R}^3.$$

187 The quotient space by this equivalence relation is not a manifold. If we ignore the degenerate
 188 volume elements of the form $(x_0, \dots, x_0)^t$ we get an open subset of \mathbb{R}^{3k}

$$M := \mathbb{R}^{3k} \setminus \{(x_0, \dots, x_0)^t \mid x_0 \in \mathbb{R}^3\}$$

189 whose quotient space M/\sim is simply (diffeomorphic to) a $(3k-4)$ -sphere. To be more concrete,
 190 the map on M/\sim induced by the projection map π in (3.3) yields an identification

$$(4.1) \quad \pi : M/\sim \longrightarrow N := \{x \in \mathbb{R}^{3k} \mid \|x\| = 1 \text{ and } x_* := \sum_{i=1}^n x_i = 0\}.$$

191 The differential structure on N induces a differential structure on M , and we can consider
 192 their tangent bundles TM and TN . These are related via the differential $D(\pi) : TM \rightarrow TN$ of
 193 π .

194 **4.2. The gradient field.** Let $C^\infty(M, TM)$ be the space of smooth sections of TM , also
 195 known as vector fields. For a tetrahedral volume element $x = (x_1, \dots, x_4)^t \in M$ it is straight-
 196 forward to compute from Equation (3.1) that the gradient ∇vol_τ of the volume function at x
 197 is given by six times the normals n_i in Equation (2.2), that is,

$$\nabla \text{vol}_\tau = \frac{1}{6} \begin{pmatrix} n_1 \\ n_2 \\ n_3 \\ n_4 \end{pmatrix}.$$

198 The gradient field $\nabla \text{vol} \in C^\infty(M, TM)$ of the volume is the vector field given by all gradient
 199 vectors $\nabla \text{vol}_x \in T_x M$ of the volume on M .

200 The factor $1/\sqrt{\|n_i\|}$ had been introduced to ensure scaling invariance. Instead, we use the
 201 factor $1/\sqrt{\|n\|}$ for $n = (n_1, \dots, n_4)^t \in \mathbb{R}^{12}$, which not only ensures scaling invariance, but also
 202 preserves the centroid. That is,

$$(4.2) \quad \tau' = \begin{pmatrix} x'_1 \\ x'_2 \\ x'_3 \\ x'_4 \end{pmatrix} := \begin{pmatrix} x_1 \\ x_2 \\ x_3 \\ x_4 \end{pmatrix} + \frac{1}{\sqrt{\|n\|}} \begin{pmatrix} n_1 \\ n_2 \\ n_3 \\ n_4 \end{pmatrix}.$$

203 The intimate relationship between the tetrahedral GETMe transformation and the gradient
 204 of the volume function allows us to generalize the tetrahedral GETMe transformation to volume
 205 elements such as hexahedra, prisms, pyramids, and even octahedra, which allows us to analyze
 206 it not only numerically, but theoretically. In particular, we show that the mean volume quality
 207 measure is a height function on the sphere N and discuss some of its properties. Notice, that a
 208 variation of the necessary scaling mentioned in §2.3 is even built into the map π given in (3.3).
 209 More precisely, we could simply leave $\|(x_1 - x_*, \dots, x_n - x_*)\|$ unchanged.

210 **5. GETMe smoothing for hybrid meshes.** In order to give a description of the GETMe
 211 smoothing, it will be helpful to discuss the theory in more detail. As we have seen, face normals
 212 play an essential role in the tetrahedral GETMe approach. After discussing face normals in more
 213 generality, we will explicitly compute gradient vector fields of the mean volume function given
 214 in Definition 3.2 for pyramids, prisms and octahedra directly from the definition. After some
 215 theory about scaling invariance and gradient vector fields, we show how to use the symmetry of
 216 Platonic solids to compute the gradient fields for other polyhedra. More precisely, we can use
 217 a symmetry-invariant subset of triangulations in order to compute the gradient. For example
 218 the hexahedron has a symmetry-invariant subset of only two triangulations.

219 **5.1. Face normals.** By the face normal of an oriented triangle we simply mean the cross
 220 product of two edge vectors compatible with the orientation. Even though cross products are
 221 usually applied to edge vectors, we can also apply the cross products to the vertex coordinates
 222 themselves, because they are points in the vector space \mathbb{R}^3 and therefore vectors themselves.
 223 In order to simplify notation, let us define face normals for arbitrary oriented polygonal curves
 224 $C(1, \dots, k)$ in \mathbb{R}^3 as shown in Figure 5.1 by

$$(5.1) \quad \begin{aligned} \nu(1, \dots, k) &:= (x_2 - x_1) \times (x_3 - x_1) + (x_3 - x_1) \times (x_4 - x_1) + \dots \\ &\quad + (x_{k-2} - x_1) \times (x_{k-1} - x_1) + (x_{k-1} - x_1) \times (x_k - x_1) \\ &= x_1 \times x_2 + x_2 \times x_3 + \dots + x_{k-1} \times x_k + x_k \times x_1. \end{aligned}$$

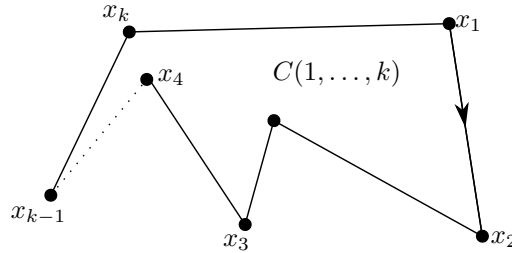


Fig. 5.1: The chain $C(1, \dots, k)$

Remark 5.1. There are several useful facts about cross products, which can be proven by elementary calculations. We have the identities

$$(5.2) \quad (x_1 - x_2) \times (x_2 - x_3) = \nu(1, 2, 3),$$

$$(5.3) \quad (x_1 - x_3) \times (x_2 - x_4) = \nu(1, 2, 3, 4),$$

$$(5.4) \quad \nu(2, \dots, k, 1) = \nu(1, \dots, k) = \sum_{j=2}^{k-1} \nu(1, j, j+1).$$

225 *The direction of the normal vector $\nu(1, 2, 3)$ can be found by a right-hand (grip) rule. Equa-*
 226 *tion (5.4) encodes the following properties of cross products:*

- 227 1. The face normals of tetrahedra add up to zero.
 228 2. If $C(1, \dots, k)$ is the boundary of a triangulated oriented surface, then the sum of their
 229 normals is independent of the choice of triangulation.
 230 3. If $C(1, \dots, k)$ is planar and convex, then $\|\nu(1, \dots, k)\|$ equals twice the area enclosed by
 231 $C(1, \dots, k)$.

232 The above remark gives a convenient way of organizing linear combinations of face normals.
 233 In particular, it allows us to write the gradient field $\nabla \text{vol} \in C^\infty(M, TM)$ of the volume as

$$(5.5) \quad \nabla \text{vol}_\tau = \frac{1}{6} \begin{pmatrix} \nu(4, 3, 2) \\ \nu(4, 1, 3) \\ \nu(4, 2, 1) \\ \nu(1, 2, 3) \end{pmatrix} \quad \text{for the tetrahedron } \tau = \begin{array}{c} x_4 \\ \diagdown \quad \diagup \\ x_1 \quad x_3 \\ \diagup \quad \diagdown \\ x_2 \end{array} .$$

234 It is straight-forward to also write the gradient of the mean volume for other volume ele-
 235 ments given in Definition 3.2 in terms of face normals. This vector field will yield a flow on the
 236 manifold of volume elements. We will see in §6 and §7 to which extent the optimizing behavior
 237 for tetrahedra can be observed and proven for more general polyhedra.

238 Let us compute the gradient ∇vol of the mean volume for the volume element x based
 239 on the pyramid. Its two triangulations in \mathcal{T}_x consist of only two tetrahedra each shown in
 240 Figure 3.1. We compute

$$(5.6) \quad \nabla \text{vol}_x = \frac{1}{12} \begin{pmatrix} \nu(5, 4, 2) + \nu(5, 4, 3, 2) \\ \nu(5, 1, 3) + \nu(5, 1, 4, 3) \\ \nu(5, 2, 4) + \nu(5, 2, 1, 4) \\ \nu(5, 3, 1) + \nu(5, 3, 2, 1) \\ 2 \cdot \nu(1, 2, 3, 4) \end{pmatrix} .$$

241 It is also straight-forward to construct the vector field for the prism, because its set of all
 242 triangulations has only six elements:

$$(5.7) \quad \nabla \text{vol}_x = \frac{1}{18} \begin{pmatrix} \nu(3, 2, 4) + \nu(2, 5, 4, 6, 3) \\ \nu(1, 3, 5) + \nu(3, 6, 5, 4, 1) \\ \nu(2, 1, 6) + \nu(1, 4, 6, 5, 2) \\ \nu(5, 6, 1) + \nu(6, 3, 1, 2, 5) \\ \nu(6, 4, 2) + \nu(4, 1, 2, 3, 6) \\ \nu(4, 5, 3) + \nu(5, 2, 3, 1, 4) \end{pmatrix} \quad \text{for the prism } \begin{array}{c} x_6 \\ \diagdown \quad \diagup \\ x_4 \quad x_5 \\ \diagup \quad \diagdown \\ x_1 \quad x_2 \\ x_3 \end{array} .$$

243 It is simpler to compute the vector field for the octahedron:

$$(5.8) \quad \nabla \text{vol}_x = \frac{1}{6} \begin{pmatrix} \nu(2, 3, 4, 5) \\ \nu(1, 5, 6, 3) \\ \nu(1, 2, 6, 4) \\ \nu(1, 3, 6, 5) \\ \nu(1, 4, 6, 2) \\ \nu(2, 5, 4, 3) \end{pmatrix} \quad \text{for } \begin{array}{c} x_1 \\ \diagdown \quad \diagup \\ x_2 \quad x_4 \\ \diagup \quad \diagdown \\ x_3 \\ x_6 \end{array} .$$

244 In order to compute the gradient field for more complicated polyhedra, we will discuss
 245 symmetry-invariant subsets of triangulations in §5.4.

246 **5.2. Scaling-invariance.** In order for the transformation determined by ∇vol to be in-
 247 variant under scaling, it can be normalized as in [46] by multiplying each face normal with the
 248 inverse of the square root of its norm. Instead, we will generalize the normalization used in
 249 Equation (4.2), which preserves the direction of vectors on M and the singularities of the vector
 250 field, which makes dynamical studies simpler.

251 **DEFINITION 5.2.** For a vector field $X \in TM$ on M let

$$\Psi(X_x) := \begin{cases} \frac{1}{\sqrt{\|X_x\|}} X_x & X_x \neq 0 \\ 0 & X_x = 0. \end{cases}$$

252 Furthermore we let $\Psi(X)$ be the vector field given by $\Psi(X)_x = \Psi(X_x)$.

253 Scaling and translation invariance of $\Psi(\nabla \text{vol})$ is equivalent to $\Psi(\nabla \text{vol})$ being a well-defined
 254 vector field on the quotient M/\sim .

255 **LEMMA 5.3.** The vector field $X = \Psi(\nabla \text{vol})$ is a vector field on the quotient M/\sim .

Proof. Recall the diffeomorphism $\pi: M/\sim \rightarrow N$ defined in (4.1). It suffices to check that
 $D(\pi)(X_x) = D(\pi)(X_{x'})$ for $x \sim x'$. Notice, that $tX_x = X_{tx}$ and $X_x = X_{x+(x_0, \dots, x_0)}$. Clearly, if
 $x' = x + (x_0, \dots, x_0)$, then $D(\pi)(X_{x'}) = D(\pi)(X_x)$. If $x' = \lambda x$ with $x_* = \sum x_i = 0$, then using
 the fact the ∇vol preserves the centroid we get

$$D(\pi)(X_{x'}) = \frac{d}{dt} \pi(\lambda x + tX_{\lambda x})|_{t=0} = \frac{d}{dt} \pi(\lambda(x + tX_x))|_{t=0} = \frac{d}{dt} \pi(x + tX_x)|_{t=0} = D(\pi)(X_x). \quad \square$$

256 **5.3. Gradient fields.** The gradient flow is an important concept and a powerful tool with
 257 many applications in topology, global analysis, dynamical systems and mathematical physics.
 258 Perelman observed in his proof of Thurston's geometrization conjecture [21], that one can
 259 interpret Hamilton's Ricci flow as a gradient flow. Morse theory [30, 6] with all its generalizations
 260 and infinite-dimensional manifestations in mathematical physics like Chern-Simons theory [48],
 261 Yang-Mills theory [4, 3, 33] and other gauge theories deduces topological information from the
 262 study of the singularities and the flow of a gradient field. It is a natural consequence of the strong
 263 results surrounding gradient fields and their flows, that we should make use of them to shed
 264 some light on the dynamics on the transformation given in [46] and generalize it. In this section
 265 we will discuss some important properties of gradient fields and Lyapunov functions. Most
 266 importantly, we will see, that the (normalized) gradient flow lines start and end at singularities
 267 of the gradient field.

268 Recall the quality measure $q = \text{vol} \circ \pi: M \rightarrow \mathbb{R}$ defined in (3.4). For $X_x \in T_x N$ we compute
 269 for the differential D of the mean volume $D \text{vol}(X_x) = D(\text{vol}|_N)(X_x)$. Then the gradient field
 270 $\nabla(\text{vol}|_N)$ of $\text{vol}|_N$ is implicitly defined using the submanifold metric $\langle \cdot, \cdot \rangle_N$ on $N \subset M \subset \mathbb{R}^{3k}$
 271 by

$$D \text{vol}(X_x) = \langle \nabla(\text{vol}|_N)_x, X_x \rangle_N \quad \text{for all } X_x \in T_x N.$$

272 **DEFINITION 5.4.** A smooth function $f: N \rightarrow \mathbb{R}$ is a Lyapunov function for a vector field
 273 $X \in C^\infty(N, TN)$, if

- 274 1. $Df_x(X) > 0$ for all non-singular points x ,
- 275 2. $Df_x(X) = 0$ if and only if x is a singular point of X .

276 A special case of a Lyapunov function is a smooth map $f: N \rightarrow \mathbb{R}$ and its gradient field ∇f ,
 277 because $Df_x(\nabla f) = \|\nabla f_x\|_N^2 > 0$ for all non-singular points x and $Df_x(X) = \langle \nabla f_x, X \rangle_N = 0$
 278 for all $X \in T_x N$. Since N is a compact manifold, all vector fields on N are complete: If X is a
 279 vector field, then the flow curve $\gamma(t)$ defined by the initial value problem

$$\gamma(0) = x \text{ and } \dot{\gamma}(t) = X_{\gamma(t)}$$

281 exists for all $x \in N$ and $t \in \mathbb{R}$. Let us reprove a simple fact about Lyapunov functions on
 282 compact manifolds.

283 PROPOSITION 5.5. *Let f be a Lyapunov function on N for $X \in C^\infty(N, TN)$, then the flow
 284 lines of X start and end at singularities of X .*

285 *Proof.* If γ is a flow line of X on N with $\gamma(0) = x$ and $\gamma(t_0)$ a non-singular point,

$$\frac{d}{dt}(f \circ \gamma)|_{t=t_0} = Df_{\gamma(t_0)}(X) > 0$$

286 implies that $f \circ \gamma$ is increasing for all t . Since N is compact and f continuous, $\text{Im}(f \circ \gamma)$ is a
 287 bounded set. As $f \circ \gamma$ is always increasing, but bounded, we have

$$\lim_{t_0 \rightarrow \pm\infty} \frac{d}{dt}(f \circ \gamma)|_{t=t_0} = 0.$$

288 By compactness we can furthermore find $x \in N$ and a sequence $t_n \in \mathbb{R}$ such that

$$\lim_{n \rightarrow \infty} t_n = \infty \quad \text{and} \quad \lim_{n \rightarrow \infty} \gamma(t_n) = x \in N.$$

289 It follows that x is singular, because $Df_x(X) = \lim_{n \rightarrow \infty} \frac{d}{dt}(f \circ \gamma)|_{t=t_n} = 0$. Since X is smooth,
 290 we have $\|\dot{\gamma}(t)\| = \|X_{\gamma(t)}\| \rightarrow 0$ as $t \rightarrow \infty$, which implies

$$\lim_{t \rightarrow \infty} \gamma(t) = x.$$

291 A similar argument shows that γ starts at a singularity. \square

292 The following corollary from Proposition 5.5 describes the qualitative behavior of the flow
 293 of $D(\pi)(\nabla \text{vol})$ and $D(\pi)(\Psi(\nabla \text{vol}))$.

294 THEOREM 5.6. *The vector field $X = D(\pi)(\nabla \text{vol}) = \nabla(\text{vol}|_N)$ on N is the gradient field of
 295 $f|_N$, and the flow lines of X and $\tilde{X} = D(\pi)(\Psi(\nabla \text{vol}))$ on $N \subset M$ start and end at singularities
 296 of Y .*

297 *Proof.* We compute

$$D(\pi)\nabla \text{vol}_x = \nabla \text{vol}_x - (\nabla \text{vol}_x \cdot x) \cdot x \quad \text{for } x \in N.$$

Since $x \in N \subset \mathbb{R}^{3k}$ is orthogonal to $X_x \in T_x N \subset \mathbb{R}^{3k}$, we get

$$\begin{aligned} \langle \nabla(\text{vol}|_N)_x, X_x \rangle_N &= D \text{vol}(X_x) = \langle \nabla \text{vol}_x, X_x \rangle = \langle D(\pi)(\nabla \text{vol}_x) + (\nabla \text{vol}_x \cdot x) \cdot x, X_x \rangle \\ &= \langle D(\pi)(\nabla \text{vol}_x), X_x \rangle = \langle D(\pi)(\nabla \text{vol}_x), X_x \rangle_\pi. \end{aligned}$$

298 This shows that $D(\pi)(\nabla \text{vol})$ is the gradient field $\nabla(\text{vol}|_N)$ of $\text{vol}|_N$. In particular $\text{vol}|_N$ is a
 299 Lyapunov function for $D(\pi)(\nabla \text{vol})$.

Therefore we also have

$$D(\text{vol}|_N)_x (D(\pi)(\Psi(\nabla \text{vol}_{\gamma(t)}))) = \frac{1}{\sqrt{\nabla \text{vol}_{\gamma(t)}}} D(\text{vol}|_N)_x (D(\pi)(\nabla \text{vol}_{\gamma(t)})) > 0.$$

300 Since Ψ preserves singularities, $\text{vol}|_N$ is also a Lyapunov function for $D(\pi)(\Psi(\nabla \text{vol}))$. The
 301 theorem follows from Lemma 5.5. \square

302 We are interested in the normalization $\Psi(\nabla \text{vol})$ of ∇vol , because it is a scaling invariant
 303 vector field. One can also ask about the dynamic behavior of normalizations given by division of
 304 other powers of the norm and coordinate-wise normalizations. We expect them to have the same
 305 qualitative behavior. In the case of simply dividing by the norm of X , this dynamical behavior

306 is described in Thom's gradient conjecture [25]. The above theorem also shows that the flow of
 307 the vector fields $D(\pi)(\nabla \text{vol})$ and $D(\pi)(\Psi \nabla \text{vol})$ optimize the quality measure $q = \text{vol} \circ \pi$. See
 308 [40] how one can turn this observation into an efficient and global optimization-based smoothing
 309 method.

310 The vector fields $D(\pi)(\nabla \text{vol})$ and $D(\pi)(\Psi \nabla \text{vol})$ therefore have the same singularities and
 311 qualitative behavior as described Theorem 5.6. This suggests that the two vector fields are
 312 topologically equivalent, that is, there is a homeomorphism $N \rightarrow N$ carrying trajectories to
 313 trajectories and preserving the direction of increasing time. However, we do not see, how to
 314 prove such a strong result. Since the kernel of $D(\pi)_x: \mathbb{R}^{3n} \rightarrow T_x N$ consists of the radial
 315 vectors, that is, vectors of the form λx , the singularities of these vector fields have the following
 316 characterization in terms of vol.

317 LEMMA 5.7. *The vector field $D(\pi)(\text{vol})$ on $N \subset M$ has a singularity at $x \in N$ if and only*
 318 *if*

$$(5.9) \quad \lambda x = \nabla \text{vol}_x \text{ for some constant } \lambda \in \mathbb{R}.$$

319

320 **5.4. Symmetry.** Mani [28] showed that for each polyhedral graph G , there exists a convex
 321 polyhedron P_G such that every automorphism of G is induced by an isometry of Euclidean space.
 322 We call P_G a *symmetric* polyhedron. Examples for symmetric polyhedra include the platonic
 323 solids, semi-regular polyhedra, the right regular prism, right regular anti-prism and the regular
 324 pyramid. In this section every polyhedron P is assumed to be symmetric.

325 Consider the *symmetry group* Γ of a (symmetric) polyhedron $P \subset \mathbb{R}^3$ as a subgroup of
 326 isometry group of \mathbb{R}^3 , that fixes P . Therefore, $g \in \Gamma$ acts on all points in $p \in \mathbb{R}^3$ as usual by
 327 $g \cdot p \in \mathbb{R}^3$. In particular, it naturally acts on a triangulation T of P , and we can consider a Γ -
 328 invariant subset $\mathcal{T}' \subset \mathcal{T}$ of triangulations of polyhedra. In this way, a Γ -invariant triangulation
 329 of a polyhedron gives a simpler definition of the mean volume in Definition 3.2

$$\text{vol}(x) = \frac{1}{|\mathcal{T}'_x|} \sum_{T \in \mathcal{T}'_x} \sum_{\tau \in T} \text{vol}(\tau).$$

330 Notice, that the orbit of an arbitrary triangulation under Γ yields a Γ -invariant subset of all
 331 triangulations.

332 Let us consider the two possible triangulations of the hexahedron consisting of 5 tetrahedra
 333 each and apply this theorem to this Γ -invariant subset \mathcal{T} of all triangulations.

$$(5.10) \quad X_p^{\mathcal{T}} = \frac{1}{12} \begin{pmatrix} \nu(2, 5, 4) + \nu(6, 5, 8, 4, 3, 2) \\ \nu(3, 6, 1) + \nu(7, 6, 5, 1, 4, 3) \\ \nu(4, 7, 2) + \nu(8, 7, 6, 2, 1, 4) \\ \nu(1, 8, 3) + \nu(5, 8, 7, 3, 2, 1) \\ \nu(1, 6, 8) + \nu(6, 7, 8, 4, 1, 2) \\ \nu(2, 7, 5) + \nu(7, 8, 5, 1, 2, 3) \\ \nu(3, 8, 6) + \nu(8, 5, 6, 2, 3, 4) \\ \nu(4, 5, 7) + \nu(5, 6, 7, 3, 4, 1) \end{pmatrix} \quad \text{for} \quad \begin{array}{c} \begin{array}{c} x_8 \\ \diagup \quad \diagdown \\ x_5 \quad x_7 \\ \diagdown \quad \diagup \\ x_4 \quad x_6 \\ \diagup \quad \diagdown \\ x_1 \quad x_2 \\ \diagdown \quad \diagup \\ x_3 \end{array} \end{array}.$$

334 In addition to the hexahedron, it is now a straight-forward task to write down and check
 335 gradient fields for the rest of the platonic solids. In §6.6 we mention a gradient field for the
 336 icosahedron, which is a variation of the gradient field of the mean volume. We leave the
 337 explicit gradient field for the dodecahedron to the interested reader, because the expression is
 338 considerably longer.

339 **5.5. Smoothing of hybrid meshes.** We have constructed elementary transformations
 340 for tetrahedra, hexahedra, pyramids, prisms and octahedra. We will see in §6 and §7, that
 341 they make individual volume elements more regular. Moreover, we will single out the vector
 342 fields, which exhibit the fastest convergence for each each of the four main volume elements
 343 and provide numerical tests in Figure 7.2. Using the corresponding GETMe transformations,
 344 we get a smoothing algorithm for hybrid meshes as described in §2.3, whose performance we
 345 compare to the original results from GETMe transformations in §7.

346 **6. Regularity.** Intuitively, symmetry and regularity are related notions. One definition
 347 found in the literature is, that a polyhedron is regular, if the action of its symmetry group
 348 acts transitively on its flags, so that the platonic solids are the only regular, convex polyhedra
 349 [15]. A flag is a connected set of elements of each dimension—for a polyhedron that is the
 350 body, a face, an edge of the face, a vertex of the edge, and the null polytope. Nevertheless,
 351 prisms and pyramids are also sometimes called regular, if they are symmetric. This notion can
 352 also be extended to isogonal polytopes, that is, polytopes, for which their symmetry group acts
 353 transitively on its vertices. Let us therefore call a pyramid, a prism and an isogonal polyhedron
 354 regular, if it is symmetric (and convex). It has been observed heuristically in [39], that the
 355 iterative application of certain actions induced by the symmetry group on polygons regularizes
 356 them. In a way this is our hope for the flow of the gradient fields of the mean volume for a
 357 Γ -invariant set of triangulations \mathcal{T} . In this section, we will discuss this in more detail.

358 In the case of tetrahedra, we will show directly in §6.1 that the non-collinear singularities
 359 are regular tetrahedra. In particular we see by Table 7.1, that the positively oriented one is a
 360 sink, and the negatively oriented one is a source of the gradient flow.

361 It is tempting to think that this generalizes to other polyhedra with non-vanishing mean
 362 volume, namely that the singularities of the mean volume flow on N are regular polyhedra in
 363 some sense. Unfortunately, this naive approach will only work for rather simple polyhedra, even
 364 if they have a large symmetry group. For example, in the case of the icosahedron, there are a
 365 lot more singularities of the mean volume function than just the regular icosahedron, and, in
 366 particular, the regular icosahedron does not maximize the mean volume function on N . In this
 367 case, a slightly more complicated gradient field seems to have the desired symmetric icosahedra
 368 as singularities: the regular icosahedron and the great icosahedron (one of the Kepler–Poinset
 369 polyhedra).

370 While we have confirmed numerically, that the gradient flow of the mean volume exhibits a
 371 regularizing dynamic behavior for the tetrahedron, the pyramid, the octahedron, the hexahedron
 372 and even the dodecahedron, we can rigorously confirm this behavior only for the tetrahedron,
 373 the pyramid and the octahedron. For the hexahedron, we can show it for a slightly different
 374 gradient field. Surprisingly and regrettably, we have not yet been able to prove it for the prism,
 375 even though numerical tests, in particular a computation of the eigenvalues of the Hessian of the
 376 collinear prisms, suggest, that the mean volume is a Morse-Bott function just like we prove it for
 377 tetrahedra in §7.1. The icosahedron and the dodecahedron have only been studied numerically.

378 Based on Lemma 5.7 we make the following definition:

379 **DEFINITION 6.1.** *Let X be a vector field on $N = M/\sim$ given by a linear combination of*
 380 *cross products. The volume element x is X -optimal, if there exists $y \sim x$ satisfying*

$$(6.1) \quad \lambda y = X_y \quad \text{for some } \lambda \neq 0.$$

381 *In particular, no collinear x is X -optimal. The sign of λ determines the orientation of x .*

382 We expect that the X -optimal volume elements are sinks or sources depending on the sign
 383 of λ . It is difficult in general to determine the shape of the singularities. Let us therefore discuss
 384 X -optimality for the platonic solids, the prism and the pyramid, when X is the gradient of the
 385 mean volume or a slight variation of it.

386 **6.1. The tetrahedron.** The tetrahedron is the simplest case. We show in §7.1, that the
 387 mean volume is a Morse-Bott function on the sphere N . In particular, the dynamics of its
 388 gradient flow are well-understood, see §7.

389 **THEOREM 6.2.** *The non-collinear singularities of the gradient of the (mean) volume for*
 390 *tetrahedra are regular tetrahedra.*

391 *Proof.* Consider the gradient ∇vol of the volume given in (5.5). If x is a non-collinear
 392 singularity, it is (∇vol) -optimal. Let us assume without loss of generality that $x_4 = 0$. Then

$$\frac{6\lambda}{2}(x_1 - x_2) = \frac{1}{2}(\nu(4, 3, 2) - \nu(4, 1, 3)) = x_3 \times \left(\frac{1}{2}(x_1 + x_2) \right).$$

393 Therefore $x_1 - x_2$ is orthogonal to the hyperplane spanned by x_3 and $\frac{1}{2}(x_1 + x_2)$. In particular,
 394 the face with vertices x_1 , x_2 and x_3 is isosceles, see Figure 6.1. By symmetry, all edges of the
 tetrahedron are of equal length, and therefore the tetrahedron is regular. \square

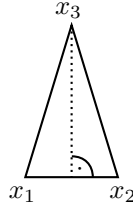


Fig. 6.1: Isosceles triangle

395

396 **6.2. The pyramid.** Consider the gradient (∇vol) of the mean volume function for pyra-
 397 mids given in (5.6). Suppose x is ∇vol -optimal. We compute $x_4 - x_3 = x_2 - x_1$. Therefore the
 398 base of a singularity is a (planar) parallelogram. Furthermore if $\lambda x = X_x$ for $\lambda \neq 0$ then

$$\frac{12\lambda}{2}(x_2 + x_4) = \nu(4, 3, 2, 1) \quad \text{and} \quad \frac{12\lambda}{2}(x_1 + x_3) = \nu(4, 3, 2, 1).$$

Therefore x_5 lies vertically above the center of the parallelogram base. Now consider

$$\begin{aligned} 12\lambda(x_4 - x_1) &= \nu(5, 3, 1) + \nu(5, 3, 2, 1) - \nu(5, 4, 2) - \nu(5, 4, 3, 2) \\ &= \nu(5, 3, 1) + \nu(5, 2, 4) + \nu(5, 2, 1) + \nu(5, 3, 4). \end{aligned}$$

399 We observe that for some constant C

$$\nu(5, 3, 1) + \nu(5, 2, 4) = C(x_4 - x_1)$$

400 and

$$(\nu(5, 2, 1) + \nu(5, 3, 4)) \perp x_2 - x_1.$$

Since x is non-collinear, the base is a parallelogram and x_5 does not lie in the base, we have $\nu(5, 2, 1) + \nu(5, 3, 4) \neq 0$. We conclude that $x_4 - x_1$ and $x_2 - x_1$ are nonzero and orthogonal to each other. If we translate x so that $x_5 = 0$ we get

$$\begin{aligned} 12\lambda(x_4 - x_2) &= 2\nu(5, 3, 1) + \nu(5, 3, 2, 1) + \nu(5, 3, 4, 1) \\ &= 2x_3 \times x_1 + (x_3 - x_1) \times (x_2 + x_4) \\ &= (x_3 - x_1) \times (x_1 + x_3 + x_2 + x_4). \end{aligned}$$

401 The right-hand side is orthogonal to $x_3 - x_1$. Therefore, the base is a square, and x is a
 402 symmetric pyramid, whose height is determined by the following result.

403 **THEOREM 6.3.** *Every (∇vol) -optimal pyramid is of the form $\pi(x) \in N$, where*

$$x = \begin{pmatrix} (0, 0, 0) \\ (2, 0, 0) \\ (2, 2, 0) \\ (0, 2, 0) \\ (1, 1, \sqrt{5}) \end{pmatrix}.$$

404

Proof. Consider a pyramid of height h with square base of area a^2 and apex orthogonally above the middle of the base. If x is (∇vol) -optimal, then we compute $\|\nu(1, 2, 3, 4)\| = 2a^2$ and $\|\nu(5, 2, 4)\| = h \cdot \|x_4 - x_2\|$. For $\lambda \neq 0$ as in Definition 6.1 we have

$$24\lambda h = 24\lambda \left\| x_5 - \frac{x_1 + x_2 + x_3 + x_4}{4} \right\| = \|2\nu(1, 2, 3, 4) - \frac{1}{2}\nu(4, 3, 2, 1)\| = 5a^2$$

$$\text{and } 24\lambda \|x_3 - x_1\| = \|4\nu(5, 2, 4) + \nu(2, 1, 4) + \nu(3, 4, 2)\| = 4h \|x_4 - x_2\|.$$

405 Since $\|x_3 - x_1\| = \|x_4 - x_2\|$, we compute

$$\frac{h}{a} = \frac{\sqrt{5}}{2}. \quad \square$$

406 *Remark 6.4.* From the perspective of the finite element method, it is desirable, that all
 407 edges have the same length. We have two options to take care of this issue. We can ignore it
 408 entirely by arguing, that the edges connected with the apex for x as in Theorem 6.3 have length
 409 $\sqrt{7} \approx 2.64575$, which might be close enough to 2 for mesh smoothing applications. Alternatively,
 410 if we are willing to let go of the theoretical advantages of a gradient field, it is straight-forward
 411 to vary the vectors in the gradient field so that all edges have the same length and the optimal
 412 singularities are preserved. Clearly, we have a lot of (topologically) equivalent transformations
 413 at our disposal and we can control the shape of the optimal pyramid, if we could only prove
 414 topological equivalence of the corresponding vector fields.

415 **6.3. The octahedron.** Consider the gradient ∇vol of the mean volume for the octahedron
 416 given in Equation (5.8). Let x be a (∇vol) -optimal volume based element based. Then we can
 417 readily calculate that $x_3 - x_6 = x_1 - x_5$. Together with analogous statements for the other
 418 edges, we see that $C(2, 3, 4, 5)$ and the other equator curves are a parallelograms. Furthermore,
 419 $x_1 - x_6 = 2\nu(2, 3, 4, 5)$, therefore $x_1 - x_6$ is orthogonal to the plane, in which $C(2, 3, 4, 5)$ lies.
 420 Together with the analogous statements for the other cases this implies orthogonality of the
 421 planes, in which $C(2, 3, 4, 5)$, $C(1, 2, 6, 4)$ and $C(1, 3, 6, 5)$ lie.

To prove the regularity of the octahedron, it remains to check that the area of the rhombi circumscribed by $C(2, 3, 4, 5)$, $C(1, 2, 6, 4)$ and $C(1, 3, 6, 5)$ are all equal. We compute

$$\begin{aligned} \|\nu(1, 3, 6, 5)\| &= \frac{1}{2} \|x_1 - x_6\| \cdot \|x_3 - x_5\| = \frac{(6\lambda)^{-2}}{2} \|2\nu(2, 3, 4, 5)\| \cdot \|\nu(1, 2, 6, 4) - \nu(1, 4, 6, 2)\| \\ &= 2(6\lambda)^{-2} \|\nu(2, 3, 4, 5)\| \cdot \|\nu(1, 2, 6, 4)\|. \end{aligned}$$

422 By symmetry we also have $\|\nu(2, 3, 4, 5)\| = 2(6\lambda)^{-2} \|\nu(1, 3, 6, 5)\| \cdot \|\nu(1, 2, 6, 4)\|$. Therefore, once
 423 again by symmetry,

$$\|\nu(2, 3, 4, 5)\| = \|\nu(1, 3, 6, 5)\| = \|\nu(1, 2, 6, 4)\| = \frac{1}{2}(6\lambda)^2.$$

424 This shows the following.

425 **THEOREM 6.5.** *Every (∇vol) -optimal x is a regular octahedron.*

426 **6.4. The prism.** We are in a bit of a dilemma in the case of the prism. We have not
 427 been able to determine the singularities of the gradient ∇vol of the mean volume on N given
 428 in Equation (5.7). The computation of the optimal singularities for the simpler vector field

$$(6.2) \quad Y_x = \begin{pmatrix} \nu(3, 2, 5, 4, 6) \\ \nu(1, 3, 6, 5, 4) \\ \nu(2, 1, 4, 6, 5) \\ \nu(5, 6, 3, 1, 2) \\ \nu(6, 4, 1, 2, 3) \\ \nu(4, 5, 2, 3, 1) \end{pmatrix}$$

429 is straight-forward. Let x be Y -optimal. Then we have $x_3 - x_6 = x_2 - x_5$ and analogous
 430 equations for the other quadrilateral facets. This proves that the quadrilateral facets are paral-
 431 lelograms. Therefore $\nu(1, 2, 3) = -\nu(4, 5, 6)$ and $\lambda(x_1 - x_4) = \nu(1, 2, 3) - \nu(4, 5, 6) = 2\nu(1, 2, 3)$.
 432 Every Y -optimal x is therefore a symmetric prism of a certain height. Our dilemma is that we
 433 can only prove half of the facts necessary for a complete picture of the dynamics of ∇vol and Y :
 434 Unfortunately Y is not a gradient vector field, as can be checked by the integrability theorem,
 435 but ∇vol is; on the other hand, we know the singularities of Y , but not of ∇vol . Based on
 436 numerical tests we conjecture, that Y is topologically equivalent to ∇vol . This would solve our
 437 dilemma.

438 Assuming that ∇vol and Y have the same number of optimal singularities, the following
 439 result determines all ∇vol -optimal x .

440 **THEOREM 6.6.** *Every symmetric ∇vol -optimal prism is of the form $\pi(x) \in N$, where*

$$x = \begin{pmatrix} (0, 0, 0) \\ (2, 0, 0) \\ (1, \sqrt{3}, 0) \\ (0, 0, \sqrt{\frac{8}{3}}) \\ (2, 0, \sqrt{\frac{8}{3}}) \\ (1, \sqrt{3}, \sqrt{\frac{8}{3}}) \end{pmatrix}.$$

441 *Proof.* Consider a prism with equilateral triangles for the base faces and rectangles for
 442 the other three faces, where $x \in N$. Let a be the length of each side of the bases, and let h
 443 be the height of the prism. Therefore the area of each base is $\sqrt{3}a^2/4$, and the area of each
 444 rectangular face is $h \cdot a$. The prism $x \in N$ is ∇vol -optimal, if and only if it is X -optimal, where
 445 $X = 18\nabla \text{vol}$. Therefore, let $\lambda x = X$. We have

$$(6.3) \quad \begin{aligned} \lambda a &= \lambda \|x_3 - x_2\| = \|X_{x_3} - X_{x_2}\| = 2H \cos\left(\frac{\pi}{6}\right) \\ &= H\sqrt{3}, \quad \text{where } H = \frac{3}{2}h \cdot a \end{aligned}$$

447 and

$$\lambda h = \lambda \|x_4 - x_1\| = \|X_{x_4} - X_{x_1}\| = a^2\sqrt{3}.$$

448 The argument behind Equation (6.3) is indicated in Figure 6.2; an elementary calculation
 449 shows that the length $2H$ of the projections of $2X_{x_3} = \nu(2, 1, 6) + \nu(1, 4, 6, 5, 2)$ and $2X_{x_2} =$
 450 $\nu(1, 3, 5) + \nu(3, 6, 5, 4, 1)$ to the base each agrees with 3 times the area of each rectangular face.
 451 It follows that

$$\frac{h}{a} = \sqrt{\frac{2}{3}}. \quad \square$$

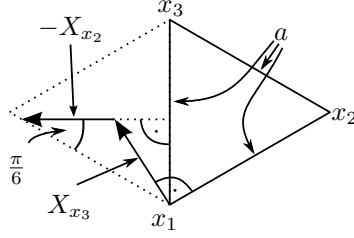


Fig. 6.2: The projection of the prism to the base

452

453

454

455

456

457

Remark 6.7. As in the case of the pyramid, a prism with all edges of the same length might be more desirable. It is straight-forward to construct a non-gradient field from the gradient field, such that the optimal singularities have the desired edge-length.

6.5. The hexahedron. We have not been able to compute the optimal polyhedra for the gradient of the mean volume given in Equation (5.10). However, the vector field

$$(6.4) \quad Y_x = \frac{1}{2} \begin{pmatrix} \nu(3, 6, 8) + \nu(2, 5, 4) + \nu(6, 5, 8, 4, 3, 2) \\ \nu(4, 7, 5) + \nu(3, 6, 1) + \nu(7, 6, 5, 1, 4, 3) \\ \nu(1, 8, 6) + \nu(4, 7, 2) + \nu(8, 7, 6, 2, 1, 4) \\ \nu(2, 5, 7) + \nu(1, 8, 3) + \nu(5, 8, 7, 3, 2, 1) \\ \nu(2, 7, 4) + \nu(1, 6, 8) + \nu(6, 7, 8, 4, 1, 2) \\ \nu(3, 8, 1) + \nu(2, 7, 5) + \nu(7, 8, 5, 1, 2, 3) \\ \nu(4, 5, 2) + \nu(3, 8, 6) + \nu(8, 5, 6, 2, 3, 4) \\ \nu(1, 6, 3) + \nu(4, 5, 7) + \nu(5, 6, 7, 3, 4, 1) \end{pmatrix}$$

458

459

differs from the gradient of the mean volume only slightly and is still a gradient field: If $\tau_1(x) = (x_3, x_6, x_8, x_1)$ and $\tau_2(x) = (x_2, x_4, x_5, x_7)$, then we have

$$Y_x = 6\nabla f_x^Y \quad \text{for } f^Y \equiv \text{vol} + \frac{1}{2} \text{vol} \circ \tau_1 + \frac{1}{2} \text{vol} \circ \tau_2.$$

460

461

462

In order to compute the optimal singularities, let us denote the faces by A_i and the corresponding face normals by n_i , $i = 1, \dots, 8$ given by the cross product of the diagonals as indicated in Figure 6.3.

463

464

465

466

467

468

469

It is straight-forward to compute $x_1 - x_4 = x_5 - x_8$ for any Y -optimal polyhedron x . It follows that $x_1 - x_8 = (x_4 - x_8) + (x_5 - x_8)$, so that A_3 is planar. By symmetry every singularity has planar faces. It also follows from $x_1 - x_4 = x_5 - x_8$ that $A_i \parallel A_{i+3}$ for $i = 1, 2, 3$.

Furthermore, we have $\lambda(x_4 - x_8) = n_1 + \nu(2, 5, 7) - n_4 - \nu(1, 6, 3)$. Notice that $(\nu(2, 5, 7) - \nu(1, 6, 3)) \parallel n_1$, so that $(x_4 - x_8) \parallel n_1$ and the faces A_3 and A_1 are orthogonal to each other. By symmetry the same is true for the other faces. Such an element is known as an orthotope.

For an orthotope it is straight-forward to see that

$$\frac{1}{2}(n_1 + n_2 + n_3) = \nu(3, 6, 8).$$

470

Therefore, the first entry of Y_x satisfies

$$\nu(6, 5, 8, 4, 3, 2) = \frac{1}{2}(n_1 + n_2 + n_3) + \nu(2, 5, 4) = \nu(2, 5, 4) + \nu(3, 6, 8),$$

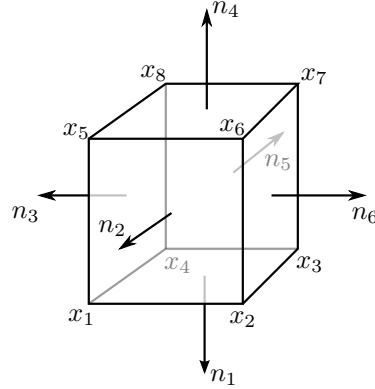


Fig. 6.3: The face normals of the hexahedron

471 and the analogous relation holds for the other entries. Let us compute the area of A_3 of our
 472 orthotope in two equivalent ways. On the one hand the area is simply $\|n_3\|$, on the other hand
 473 it is $\|x_4 - x_8\| \cdot \|x_5 - x_8\|$. It follows that

$$\|n_3\| = 4\lambda^2 \|n_1 - n_4\| \cdot \|n_2 - n_5\| = 16\lambda^2 \|n_1\| \cdot \|n_2\|.$$

474 By symmetry we have $\|n_1\| = 16\lambda^2 \|n_2\| \cdot \|n_3\|$ and therefore $\|n_3\| = 16^2 \lambda^4 \|n_2\|^2 \|n_3\|$. We
 475 compute $\|n_2\| = (16\lambda)^{-2}$. By symmetry we see that $\|n_1\| = \|n_2\| = \|n_3\| = (16\lambda)^{-2}$. Therefore
 476 every optimal singularity is a cube.

477 **6.6. The icosahedron and the dodecahedron.** Due to its triangular faces the i -th
 478 entry of the gradient X of the mean volume is given by the normal vector to the surfaces enclosed
 479 by the link of x_i . However, the singularities of the gradient flow are not only regular icosahedra.
 480 In fact, the regular icosahedra are not maximal with respect to the volume function. We can
 481 vary the gradient flow by adding the normal vector to the surfaces enclosed by the link of the
 482 point opposite to x_i . More precisely, the resulting gradient vector Y is given by Equation (6.5),
 483 where only the first entry is shown and the other entries can be found by rotation symmetry.
 484 Experiments have shown that the Y -optimal singularities are regular icosahedra and regular
 485 great icosahedra.

$$(6.5) \quad Y_x = \frac{1}{6} \begin{pmatrix} \nu(2, \dots, 6) \\ +\nu(7, \dots, 11) \\ +\nu(5, 7, 3, 10, 6, 8, 4, 11, 2, 9) \\ \vdots \end{pmatrix} \quad \text{for} \quad \begin{array}{c} x_1 \\ x_2 \quad x_3 \quad x_4 \quad x_5 \\ x_6 \quad x_7 \quad x_8 \quad x_9 \quad x_{10} \\ x_{11} \quad x_{12} \end{array} .$$

486 If X is the gradient of the mean volume for the dodecahedra, we have observed experimen-
 487 tally, that the X -optimal singularities are regular dodecahedra.

488 **7. Dynamics.** So far, we have constructed a quality measure based on the mean volume
 489 of each volume element, related its gradient to the tetrahedral GETMe smoothing algorithm,
 490 generalized it to hybrid meshes and showed theoretically that the regular volume elements are
 491 singularities of the gradient field. We are left with analyzing the dynamics, both theoretically
 492 and numerically. We will start with showing that the signed volume for tetrahedral volume

493 elements is a Morse-Bott function on the 8-sphere N , that is, a smooth function on N whose
 494 critical set is a closed submanifold and whose Hessian is non-degenerate in the normal direction.
 495 In particular this explains the qualitative behavior of its flow, even for negatively oriented
 496 tetrahedra. We will then see, what we can say about the dynamics for other volume elements
 497 from a theoretical point of view, before we provide numerical evidence.

498 **7.1. Volume as a Morse-Bott function for tetrahedra.** In general, the group $\text{SO}(3)$
 499 acts on $(x_1, \dots, x_n) \in M$ by rotating all x_i simultaneously, and the vector field ∇vol is invariant
 500 under rotation. Therefore, all critical points of the mean volume on N are degenerate due to
 501 the rotational invariance. The action of $\text{SO}(3)$ on the $(3n - 4)$ -sphere N is proper and free
 502 as long as the x_i are not collinear: The stabilizer $S_x = \{A \in \text{SO}(3) \mid x \cdot A = x\}$ for every
 503 collinear $x \in M$ is S^1 . The collinear tetrahedra consist of the n -dimensional vector space V
 504 of n ordered points on each line through the origin in \mathbb{R}^3 . These rays can be parameterized
 505 by S^2 . Since tetrahedra with all vertices having the same coordinates are excluded in M , this
 506 parametrization by S^2 is one-to-one. The map $\pi: M \rightarrow N$ first translates the n points on
 507 the ray, so that their centroid is the origin, then normalizes the result to have length 1. This
 508 corresponds to a surjection of V onto an $n - 1$ -dimensional sub-vector space W of V , followed
 509 by a projection to the $n - 2$ -dimensional unit-sphere in W . Therefore, the subspace S_c of
 510 collinear $x \in N$ is diffeomorphic to $S^2 \times S^{n-2}$ via π . Clearly, the set of singular tetrahedra with
 511 vanishing volume consists of the collinear ones and is diffeomorphic to $S^2 \times S^2$. In general, S_c
 512 is only a subset of the critical points of the mean volume.

513 In order to show that the (mean) volume on N is Morse-Bott for tetrahedra, we need to
 514 compute the eigenvalues of the Hessian. The Hessian of the volume on M is equal to the gradient
 515 of ∇vol . In order to compute the eigenvalues of the Hessian of the restriction of $\text{vol}: M \rightarrow \mathbb{R}$
 516 to N at a regular tetrahedral volume element x , we can compute the eigenvalues of the Hessian
 517 of $\text{vol} \circ \pi$ and keep in mind, that six eigenvalues are zero; three from the translation invariance,
 518 two from the rotation invariance and one from the scaling invariance. On the level of vector
 519 fields we need to take the differential $D(\pi)(X_x)$ of X_x via $D(\pi): T_x M \rightarrow T_{\pi(x)} N$ before we take
 520 the gradient. In order to compute the eigenvalues of the Hessian of $\text{vol}|_N$ at positively oriented
 521 polyhedra, we can compute the eigenvalues of the Jacobian matrix given by the gradient of
 522 $D(\pi)(X_x) \subset T_x M$. The result of this computation is summarized in Table 7.1. By symmetry,
 523 the eigenvalues for the negatively oriented polyhedra are the same, only with the opposite
 524 sign. This agrees with the observation that the mean volume has a global minimum at the
 525 negatively oriented regular polyhedron and a global maximum at the positively oriented regular
 526 polyhedron.

Type	X	n	$(\mu, m) = \text{eigenvalue } \mu \text{ of } \pi_*(\nabla X) \text{ with multiplicity } m$
tetrahedron	(5.5)	$4 \cdot 3$	$(-\frac{2}{\sqrt{27}}, 6)$
pyramid	(5.6)	$5 \cdot 3$	$(-\sqrt{\frac{5}{27}}, 6), (-\frac{\sqrt{5}}{6\sqrt{3}}, 3)$
octahedron	(5.8)	$6 \cdot 3$	$(-\sqrt{\frac{8}{27}}, 6), (-\sqrt{\frac{2}{27}}, 6)$
prism	(5.7)	$6 \cdot 3$	$(-\sqrt{\frac{2}{27}}, 6), (-\frac{\sqrt{8}}{9\sqrt{3}}, 2), (-\frac{1}{3\sqrt{6}}, 2), (-\frac{\sqrt{2}}{9\sqrt{3}}, 2)$
hexahedron	(5.10)	$8 \cdot 3$	$(-\frac{1}{\sqrt{6}}, 6), (-\frac{5}{6\sqrt{6}}, 1), (-\sqrt{\frac{2}{27}}, 3), (-\frac{1}{\sqrt{24}}, 3), (-\frac{1}{\sqrt{66}}, 5)$
hexahedron	(6.4)	$8 \cdot 3$	$(-\sqrt{\frac{32}{3}}, 6), (-\sqrt{\frac{8}{3}}, 12)$

Table 7.1: The eigenvalues of the Hessian at positively oriented regular polyhedra

527 We also compute that the Hessian at collinear tetrahedra has two positive and two negative
 528 eigenvalues. This shows that the (mean) volume is a Morse-Bott function on the 8-sphere N ,
 529 more precisely, the critical sets are submanifolds S^2 , $S^2 \times S^2$ and S^2 at the maximum, level
 530 0 and the minimum, respectively, and the Hessian is non-degenerate in the normal direction.
 531 Furthermore, the positively oriented regular tetrahedron is a sink of the gradient flow as well
 532 as of the flow of $\Psi(\nabla \text{vol})$, while the stable and unstable manifold are two-dimensional for
 533 collinear tetrahedra. Generically, almost all tetrahedra are therefore regularized by the volume
 534 gradient flow, more precisely, the set of all tetrahedra, which are regularized, is open and dense
 535 in N . Alternatively, a small perturbation of the mean volume in a neighborhood of the level 0
 536 singularities is a Morse function with two singularities consisting of the positively and negatively
 537 oriented tetrahedra. Unfortunately, for other types of polyhedra the mean volume function is
 538 not Morse-Bott in general, despite it being constructed from the tetrahedral volume.

539 **7.2. Other volume elements.** It is easy to check that regular polyhedra are (∇vol) -
 540 optimal. However, not every (∇vol) -optimal polyhedron is regular. The results in §6 describe
 541 (∇vol) -optimal singularities for some classes of polyhedra. By Theorem 5.6 the gradient flow
 542 lines begin and end at singularities. Therefore, if there are only two optimal polyhedra, then
 543 the one with positive mean volume is a sink, while the other one is a source. It follows, that
 544 every volume element with positive mean volume will be regularized.

545 In order to have a complete picture about the dynamics of the gradient flow, we would
 546 need to address the singularities with vanishing mean volume, that is, the level 0 singularities,
 547 and their stable and unstable sets. Clearly, there are a lot of (necessarily invalid) volume
 548 elements, which would flow towards level 0 singularities. However, we expect to be able to
 549 regularize most arbitrarily small perturbations of the initial volume element. This is a heuristic
 550 statement. In order to make this mathematically precise, we would have to discuss measure
 551 theory or probability theory, which would allow us to say, that the set of volume elements, which
 552 is regularized has measure one, or that the volume elements will be regularized with probability
 553 one. However, the first necessity is the computation of the level 0 singularities. We expect
 554 these singularities to be unions of submanifolds of N , and that the stable sets are also union
 555 of submanifolds. We expect the maximal dimension of the stable manifolds to be less than the
 556 dimension of N . In particular, the complement of these stable manifolds would then be open
 557 and dense in N , which suggests, that it has measure one. This has numerically been confirmed
 558 by our tests in Figure 7.2. Unfortunately, this is not so easy to prove rigorously. Already the
 559 computation of the level 0 singularities is difficult.

560 Let us demonstrate the computation of the level 0 singularities for the pyramid. Consider
 561 $\nabla \text{vol}_x = 0$ in the case of the pyramid, where x is not collinear. If $\nu(1, 2, 3, 4) = 0$ then $x_2 = x_4$
 562 or $x_1 = x_3$. Suppose that $x_2 = x_4$ and $\nu(5, 1, 3) \neq 0$, then by $0 = \nu(5, 1, 3) + \nu(5, 1, 4, 3) =$
 563 $2\nu(5, 1, 3) + \nu(1, 4, 3)$, so that $x_2 = x_4$ lies in the plane spanned by x_1, x_3 and x_5 , such that the
 564 height of the triangle $C(1, 4, 3)$ is twice the height of the triangle $C(1, 5, 3)$. Therefore the two
 565 planar constellations given in Figure 7.1 are singular pyramids.

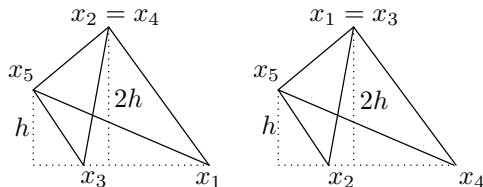


Fig. 7.1: A family of (planar) singularities for pyramids.

566 The case $\nu(1, 2, 3, 4) \neq 0$ is not possible for level 0 singularities. The submanifold of N
 567 where $\nu(1, 2, 3, 4) = 0$ and $x_1 = x_3$ is diffeomorphic to the Cartesian product of real projective
 568 3-space with the 3-sphere $\text{SO}(3) \times S^3 = \mathbb{R}P^3 \times S^3$, but it intersects other submanifolds of the
 569 singular set. Therefore the singular set is a union of three submanifolds of N , namely $S^2 \times S^3$
 570 and two copies of $\text{SO}(3) \times S^3$.

571 In applications, however, we usually do not start with volume elements of negative mean
 572 volume. In other words, if an initial mesh has volume elements negative mean volume, then
 573 we expect, that there is a problem with the setup. If we want to apply the flow to individual
 574 valid volume elements, they will have positive mean volume and can be regularized. Let us
 575 summarize the above discussion.

576 **THEOREM 7.1.** *The mean volume gradient flow regularizes volume elements based on tetra-*
 577 *hedra, pyramids and octahedra, as long as their volume is positive. The gradient flow of the*
 578 *gradient vector Y given in (6.4) regularizes all hexahedral volume elements $x \in N$ if they satisfy*
 579 *$f^Y > 0$.*

580 There are many different ways of combining this element quality measure to a sensible mesh
 581 quality measure, whose gradient flow yields simple geometric element transformations. See [40]
 582 for more information.

583 **7.3. Numerical tests.** In practice it is not important, that the vector field is actually
 584 a gradient field, therefore we have changed the vector field for the prism, the hexahedron and
 585 the pyramid slightly so that we observe faster convergence towards a regular representative. In
 586 the case of a regular pyramid and prism, we also decided that the ratio of the edges should be
 587 one. We have furthermore reduced the number of necessary cross products by making use of
 588 the centroid preserving behavior and Remark 5.1. Only the vector field for the prism is not
 589 centroid preserving. We therefore base our tests on the vector fields defined in (7.1), (7.2), (7.3)
 590 and (7.4). Each vector field $X = (X_1, \dots, X_k)$ is first multiplied by $1/\sqrt{\|X\|}$ to make it scaling-
 591 invariant, then its growth is harmonized by multiplying $X/\sqrt{\|X\|}$ by a scalar C depending on
 592 the vector field, so that $|x'_i - x'_j| = 2|x_i - x_j|$ for a regular polyhedron x and $\sigma = 1$, where

$$x' = x + \sigma \frac{C}{\sqrt{\|X\|}} X.$$

593 In the case of the tetrahedron we only need 3 cross products in the vector field

$$(7.1) \quad X_x^{\text{tet}} = \begin{pmatrix} \nu(4, 3, 2) \\ \nu(4, 1, 3) \\ \nu(4, 2, 1) \\ \nu(1, 2, 3) \end{pmatrix} = \begin{pmatrix} \nu(4, 3, 2) \\ \nu(4, 1, 3) \\ \nu(4, 2, 1) \\ -\nu(4, 3, 2) - \nu(4, 1, 3) - \nu(4, 2, 1) \end{pmatrix}$$

594 In the case of the pyramid only 5 cross products are necessary

$$(7.2) \quad X_x^{\text{pyr}} = \begin{pmatrix} \nu(5, 4, 3, 2) + 4 \cdot \nu(5, 4, 2) \\ \nu(5, 1, 4, 3) + 4 \cdot \nu(5, 1, 3) \\ \nu(5, 2, 1, 4) - 4 \cdot \nu(5, 4, 2) \\ \nu(5, 3, 2, 1) - 4 \cdot \nu(5, 1, 3) \\ 2 \cdot \nu(1, 2, 3, 4) \end{pmatrix} = \begin{pmatrix} \nu(5, 4, 3, 2) + 4 \cdot \nu(5, 4, 2) \\ \nu(5, 1, 4, 3) + 4 \cdot \nu(5, 1, 3) \\ -\nu(1, 2, 3, 4) - \nu(5, 4, 3, 2) - 4 \cdot \nu(5, 4, 2) \\ -\nu(1, 2, 3, 4) - \nu(5, 1, 4, 3) - 4 \cdot \nu(5, 1, 3) \\ 2 \cdot \nu(1, 2, 3, 4) \end{pmatrix}$$

595 For the prism 5 cross products suffice

$$(7.3) \quad X_x^{\text{pri}} = \begin{pmatrix} \nu(2, 5, 6, 3) + 3 \cdot \nu(5, 4, 6) \\ \nu(3, 6, 4, 1) + 3 \cdot \nu(5, 4, 6) \\ \nu(1, 4, 5, 2) + 3 \cdot \nu(5, 4, 6) \\ \nu(2, 5, 6, 3) + 3 \cdot \nu(1, 2, 3) \\ \nu(3, 6, 4, 1) + 3 \cdot \nu(1, 2, 3) \\ \nu(1, 4, 5, 2) + 3 \cdot \nu(1, 2, 3) \end{pmatrix}$$

In the case of the hexahedron we only need to compute 5 cross products. Given

$$\begin{aligned} X_1 &= \nu(1, 5, 8, 4) + \nu(1, 2, 6, 5) + \nu(1, 4, 3, 2), \\ X_2 &= \nu(1, 2, 6, 5) + \nu(2, 3, 7, 6) + \nu(1, 4, 3, 2), \\ X_3 &= \nu(2, 3, 7, 6) + \nu(3, 4, 8, 7) + \nu(1, 4, 3, 2), \\ X_4 &= \nu(3, 4, 8, 7) + \nu(1, 5, 8, 4) + \nu(1, 4, 3, 2), \end{aligned}$$

596 we have

$$(7.4) \quad X_x^{\text{hex}} = (X_1, X_2, X_3, X_4, -X_3, -X_4, -X_1, -X_3)^t.$$

597 For the above transformations the convergence has been tested analogously to the approach
 598 given in [44]: The tests are based on generating 100,000 random initial elements E_j of each type
 599 and taking 101 equidistant values for the scaling factor $\sigma \in [0, 1]$. For each pair (E_j, σ_k) taken
 600 from the Cartesian product of all elements and all σ -values, the geometric transformation using
 601 the scaling factor σ_k has been iteratively applied starting with the initial element E_j until the
 602 mean ratio quality number of the resulting element deviated less than 10^{-6} from the ideal value
 603 one or the number of iterations exceeded 100. For each transformation and the associated
 604 element type this test resulted in 10,100,000 transformation cycles, each represented by its
 605 number of iterations.

606 The validity of the initial element is not a necessary condition for regularization. Hence,
 607 in Figure 7.2 the results on the left are for arbitrary random nodes leading to a large amount
 608 of invalid elements (99.6% in the case of hexahedral elements). The right side depicts results
 609 for valid initial random elements. In each graph, the red line indicates the average iteration
 610 number for all 100,000 regularization cycles for a given value of σ . The boundary of the gray
 611 corridor marks the minimal and the maximal iteration numbers, hence the range of the iteration
 612 numbers for all tests. The blue corridor marks the range of the standard deviation for each
 613 value of σ .

614 In order to test and compare the performance of the resulting simultaneous and sequential
 615 GETMe smoothing for hybrid meshes, we have used the test cases and results from previous
 616 papers and compared the performance of our new smoothing algorithm for $\sigma = 1$ with the
 617 dual element-based GETMe algorithm using the same (optimized) parameters as in [45]. The
 618 results are shown in Table 7.2. The number of iterations for the two sub steps (simultane-
 619 ous/sequential), the run-times and the minimal and average mean ratio numbers are given.
 620 Figure 15 of [46] comes in 6 different flavors, three meshes with 110, 524 (S), 274, 607 (M), and
 621 400, 128 (L) tetrahedral elements in undistorted (U) and distorted (D) variants. Just like in all
 622 previous papers on GETMe smoothings, the boundary nodes have been kept fixed, which ex-
 623 plains why some examples only show poor improvements. We see, that the dual element-based
 624 and our new smoothing algorithm produce meshes of a comparable mean ratio quality in about
 625 the same amount of time. We should however note, that our algorithm is based on a different
 626 quality measure, therefore the mean ratio quality measure applied to our results is sometimes
 627 not as good as one could hope for.

628 **8. Summary and Outlook.** We have shown that the mean volume function or a variation
 629 of it can be viewed as a new, simple and geometrically intuitive regularity and quality criterion
 630 for volume elements, whose gradient flow improves the quality measured by this criterion.
 631 We have proven rigorously, that the flow regularizes the tetrahedron, the hexahedron, the
 632 pyramid and the octahedron, as long as their mean volume is positive. However, in practice
 633 this assumption is not necessary: Numerical tests show that the flow of the gradient vector field
 634 and its variations efficiently optimize and untangle the four polyhedron types, which are relevant
 635 for the finite element method. In the case of the tetrahedron, the volume function is a Morse-
 636 Bott function on S^8 , whose gradient yields the efficient smoothing algorithm introduced in [46],
 637 with one maximal and one minimal 2-sphere, as well as another set of index $(2, 2)$ singularities
 638 at level 0 homeomorphic to $S^2 \times S^2$. The mean ratio quality measure has successfully been used
 639 in order to show the effectiveness of the GETMe smoothing. The results of this paper suggest,
 640 however, that the effectiveness of GETMe would be better measured with respect to the mean
 641 volume quality measure.

In [40] we have presented an idea for constructing global optimization-based GETMe
 smoothing algorithms. During the revision process of the current work, we have found bet-
 ter algorithms based on this idea. For example, the isoperimetric quotient for polyhedra given
 by

$$\text{iq}(x) = C \frac{\text{vol}(x)}{\text{area}(x)^{3/2}},$$

describes, how round a given polyhedron $x = (x_1, \dots, x_n)$ is, where C is chosen so that
 $\max_x \text{iq}(x) = 1$. We can instead consider the difference of its enumerator and denominator

$$q(x) = \text{vol}(x) - \frac{1}{C} \text{area}(x)^{3/2}.$$

642 The functions q and iq reach their respective maxima at the same polyhedron, which can be
 643 used to construct global quality measures. If E is the set of volume elements for a mesh and x_e
 644 are the coordinates of this volume element, then we define

$$(8.1) \quad q(E) = \sum_{e \in E} q(x_e) \quad \text{and} \quad \text{iq}(E) = \prod_{e \in E} \text{iq}(x_e).$$

645 These are global quality measures with simple gradient fields, which can therefore be used for
 646 GETMe smoothing procedures as discussed in Section 2.3. Notice, that the gradient field further
 647 simplifies, because the volume function is constant for inner nodes of a mesh. Furthermore, if
 648 we fix the boundary nodes, the area function and therefore $\frac{1}{C} \text{area}(x)^{3/2}$ is a convex function.
 649 Then $q(E)$ is concave and can be used for convex optimization. A preliminary test of this
 650 idea on a planar triangle mesh using the analogous quality function corresponding to the two-
 651 dimensional isoperimetric quotient shows that this is a promising approach. As we can see in
 652 Figure 8.1, while the results from optimizing $\text{iq}(E)$ and $q(E)$ look similar, the latter makes
 653 smaller triangles worse and bigger triangles better. The function q is not scaling-invariant and
 654 favors bigger polyhedra over small polyhedra. This could theoretically lead to bad results in
 655 specific situations, but it might be no problem in practice, especially when the algorithm is
 656 combined with topology modifications to delete the triangles which are too small. In fact, the
 657 algorithm itself can help to find the small triangles, that need to be removed.

658 Even though we showed that the gradient ascent method relates the mean volume quality
 659 measure to the tetrahedral GETMe smoothing, it will be interesting to develop and analyze
 660 GETMe smoothings based on the Newton method.

661

662

663 **Acknowledgements.** We thank Joachim Wipper from TWT GmbH Science & Innovation,
 664 Department for Mathematical Research & Services, for fruitful discussions and preliminary
 665 numerical tests.

666

REFERENCES

- 667 [1] *Example Meshes by Klingner and Shewchuk*, Download:
 668 <http://www.cs.berkeley.edu/b-cam/Papers/Klingner-2007-ATM/index.html>, Accessed
 669 March 17, 2009.
- 670 [2] N. AMENTA, M. BERN, AND D. EPPSTEIN, *Optimal Point Placement for Mesh Smoothing*, Journal of
 671 Algorithms, 30 (1999), pp. 302–322.
- 672 [3] M. ATIYAH, *Collected works. Vol. 5. Gauge theories*, Oxford Science Publications, The Clarendon Press
 673 Oxford, University Press, New York, 1988.
- 674 [4] M. F. ATIYAH AND R. BOTT, *The Yang-Mills equations over Riemann surfaces*, Philos. Trans. Roy. Soc.
 675 London Ser. A, 308 (1983), pp. 523–615.
- 676 [5] F. J. BOSSEN AND P. S. HECKBERT, *A Pliant Method for Anisotropic Mesh Generation*, in Proceedings of the
 677 5th International Meshing Roundtable, 1996.
- 678 [6] R. BOTT, *Lectures on Morse theory, old and new*, Bull. Amer. Math. Soc., 7 (1982), pp. 331–358.
- 679 [7] L. V. BRANETS, *A variational grid optimization method based on a local cell quality metric*, PhD thesis,
 680 Austin, TX, USA, 2005. AAI3187661.
- 681 [8] M. BREWER, L. A. F. DIACHIN, P. M. KNUPP, T. LEURENT, AND D. MELANDER, *The Mesquite Mesh
 682 Quality Improvement Toolkit*, in Proceedings of the 12th International Meshing Roundtable, 2003,
 683 pp. 239–250.
- 684 [9] S. A. CANANN, J. R. TRISTANO, AND M. L. STATEN, *An Approach to Combined Laplacian and
 685 Optimization-Based Smoothing for Triangular, Quadrilateral, and Quad-Dominant Meshes*, in Pro-
 686 ceedings of the 7th International Meshing Roundtable, 1998, pp. 479–494.
- 687 [10] Z. CHEN, J. R. TRISTANO, AND W. KWOK, *Combined Laplacian and Optimization-based Smoothing for
 688 Quadratic Mixed Surface Meshes*, in Proceedings of the 12th International Meshing Roundtable, 2003.
- 689 [11] R. CONNELLY, *An attack on rigidity. I, II*, Bull. Amer. Math. Soc., 81 (1975), pp. 566–569.
- 690 [12] R. CONNELLY, I. SABITOV, AND A. WALZ, *The bellows conjecture*, Beiträge Algebra Geom., 38 (1997),
 691 pp. 1–10.
- 692 [13] D. E. DAVIES AND D. J. SALMOND, *Calculation of the volume of a general hexahedron for flow predictions*,
 693 AIAA Journal, 23 (1985), pp. 954–956.
- 694 [14] J. ESCOBAR, E. RODRÍGUEZ, R. MONTENEGRO, G. MONTERO, AND J. GONZÁLEZ-YUSTE, *Simultaneous
 695 untangling and smoothing of tetrahedral meshes*, Computer Methods in Applied Mechanics and Engi-
 696 neering, 192 (2003), pp. 2775 – 2787.
- 697 [15] EUCLID, *Euclid’s Elements*, Green Lion Press, Santa Fe, NM, 2002.
- 698 [16] D. A. FIELD, *Laplacian smoothing and Delaunay triangulations*, Communications in Applied Numerical
 699 Methods, 4 (1988), pp. 709–712.
- 700 [17] L. A. FREITAG, *On combining Laplacian and optimization-based mesh smoothing techniques*, in Trends in
 701 Unstructured Mesh Generation, 1997, pp. 37–43.
- 702 [18] L. A. FREITAG, M. JONES, AND P. PLASSMANN, *An Efficient Parallel Algorithm for Mesh Smoothing*, in
 703 Proceedings of the 4th International Meshing Roundtable, 1995, pp. 47–58.
- 704 [19] L. A. FREITAG AND C. OLLIVIER-GOOCH, *Tetrahedral Mesh Improvement Using Swapping and Smoothing*,
 705 International Journal for Numerical Methods in Engineering, 40 (1997), pp. 3979–4002.
- 706 [20] L. A. FREITAG AND P. PLASSMANN, *Local optimization-based simplicial mesh untangling and improvement*,
 707 International Journal of Numerical Methods in Engineering, 49 (2000), pp. 109–125.
- 708 [21] B. KLEINER AND J. LOTT, *Notes on Perelman’s papers*, Geom. Topol., 12 (2008), pp. 2587–2855.
- 709 [22] B. M. KLINGNER AND J. R. SHEWCHUK, *Aggressive Tetrahedral Mesh Improvement*, in Proceedings of the
 710 16th International Meshing Roundtable, 2007, pp. 3–23.
- 711 [23] P. M. KNUPP, *Algebraic mesh quality metrics*, SIAM J. Sci. Comput., 23 (2001), pp. 193–218.
- 712 [24] P. M. KNUPP, *Hexahedral and Tetrahedral Mesh Untangling*, Engineering with Computers, 17 (2001),
 713 pp. 261–268.
- 714 [25] K. KURDYKA, T. MOSTOWSKI, AND A. PARUSIŃSKI, *Proof of the gradient conjecture of R. Thom*, Ann. of
 715 Math. (2), 152 (2000), pp. 763–792.
- 716 [26] J. LENG, G. XU, Y. ZHANG, AND J. QIAN, *A Novel Geometric Flow-Driven Approach for Quality Improve-
 717 ment of Segmented Tetrahedral Meshes*, in Proceedings of the 20th International Meshing Roundtable,

- 718 W. R. Quadros, ed., Springer Publishing Company, Incorporated, 2012, pp. 347–364.
- 719 [27] T. LI, S. WONG, Y. HON, C. ARMSTRONG, AND R. MCKEAG, *Smoothing by optimisation for a quadrilateral*
720 *mesh with invalid elements*, *Finite Elements in Analysis and Design*, 34 (2000), pp. 37 – 60.
- 721 [28] P. MANI, *Automorphismen von polyedrischen Graphen*, *Math. Ann.*, 192 (1971), pp. 279–303.
- 722 [29] G. MEI, J. C. TIPPER, AND N. XU, *The Modified Direct Method: An Iterative Approach for Smoothing*
723 *Planar Meshes*, in *ICCS*, 2013, pp. 2436–2439.
- 724 [30] M. MORSE, *The calculus of variations in the large*, vol. 18 of *American Mathematical Society Colloquium*
725 *Publications*, American Mathematical Society, Providence, RI, 1996.
- 726 [31] S. J. OWEN, *A Survey of Unstructured Mesh Generation Technology*, in *Proceedings of the 7th International*
727 *Meshing Roundtable*, 1998, pp. 239–267.
- 728 [32] V. PARTHASARATHY AND S. KODIYALAM, *A constrained optimization approach to finite element mesh*
729 *smoothing*, *Finite Elements in Analysis and Design*, 9 (1991), pp. 309 – 320.
- 730 [33] V. RUBAKOV, *Classical theory of gauge fields*, Princeton University Press, Princeton, NJ, 2002.
- 731 [34] I. K. SABITOV, *The volume as a metric invariant of polyhedra*, *Discrete Comput. Geom.*, 20 (1998),
732 pp. 405–425.
- 733 [35] S. P. SASTRY AND S. M. SHONTZ, *Performance characterization of nonlinear optimization methods for*
734 *mesh quality improvement*, *Eng. with Comput.*, 28 (2012), pp. 269–286.
- 735 [36] K. SHIMADA, A. YAMADA, AND T. ITOH, *Anisotropic Triangulation of Parametric Surfaces via Close*
736 *Packing of Ellipsoids*, *Internat. J. Comput. Geom. Appl.*, 10 (2000), pp. 417–440. Selected papers
737 from the Sixth International Meshing Roundtable, Part II (Park City, UT, 1997).
- 738 [37] K. SHIVANNA, N. GROSLAND, AND V. MAGNOTTA, *An Analytical Framework for Quadrilateral Surface*
739 *Mesh Improvement with an Underlying Triangulated Surface Definition*, in *Proceedings of the 19th*
740 *International Meshing Roundtable*, S. Shontz, ed., Springer Berlin Heidelberg, 2010, pp. 85–102.
- 741 [38] G. STRANG AND G. FIX, *An analysis of the finite element method*, Wellesley-Cambridge Press, Wellesley,
742 MA, second ed., 2008.
- 743 [39] D. VARTZIOTIS, *Analytische Gruppentheorie und Symmetrie-Transformationen*, Unpublished manuscript,
744 (2008).
- 745 [40] D. VARTZIOTIS AND B. HIMPEL, *Efficient and global optimization-based smoothing methods for mixed-*
746 *volume meshes*, in *Proceedings of the 22nd International Meshing Roundtable*, J. Sarrate and
747 M. Staten, eds., Springer International Publishing, 2014, pp. 293–311.
- 748 [41] D. VARTZIOTIS AND M. PAPADRAKAKIS, *Improved GETMe by adaptive mesh smoothing*, *Computer Assisted*
749 *Methods in Engineering and Science*, 20 (2013), pp. 55–71.
- 750 [42] D. VARTZIOTIS AND J. WIPPER, *The Geometric Element Transformation Method for Mixed Mesh Smooth-*
751 *ing*, *Eng. Comput.*, 25 (2009), pp. 287–301.
- 752 [43] D. VARTZIOTIS AND J. WIPPER, *A dual element based geometric element transformation method for all-*
753 *hexahedral mesh smoothing*, *Comput. Methods Appl. Mech. Engrg.*, 200 (2011), pp. 1186–1203.
- 754 [44] D. VARTZIOTIS AND J. WIPPER, *Fast smoothing of mixed volume meshes based on the effective geometric*
755 *element transformation method*, *Comput. Methods Appl. Mech. Engrg.*, 201/204 (2012), pp. 65–81.
- 756 [45] D. VARTZIOTIS, J. WIPPER, AND M. PAPADRAKAKIS, *Improving mesh quality and finite element solution*
757 *accuracy by GETMe smoothing in solving the Poisson equation*, *Finite Elem. Anal. Des.*, 66 (2013),
758 pp. 36–52.
- 759 [46] D. VARTZIOTIS, J. WIPPER, AND B. SCHWALD, *The geometric element transformation method for tetrahedral*
760 *mesh smoothing*, *Comput. Methods Appl. Mech. Engrg.*, 199 (2009), pp. 169–182.
- 761 [47] T. J. WILSON, *Simultaneous Untangling and Smoothing of Hexahedral Meshes*, master’s thesis, Universitat
762 Politècnica de Catalunya, Spain, 2011.
- 763 [48] E. WITTEN, *Quantum field theory and the Jones polynomial*, *Comm. Math. Phys.*, 121 (1989), pp. 351–399.

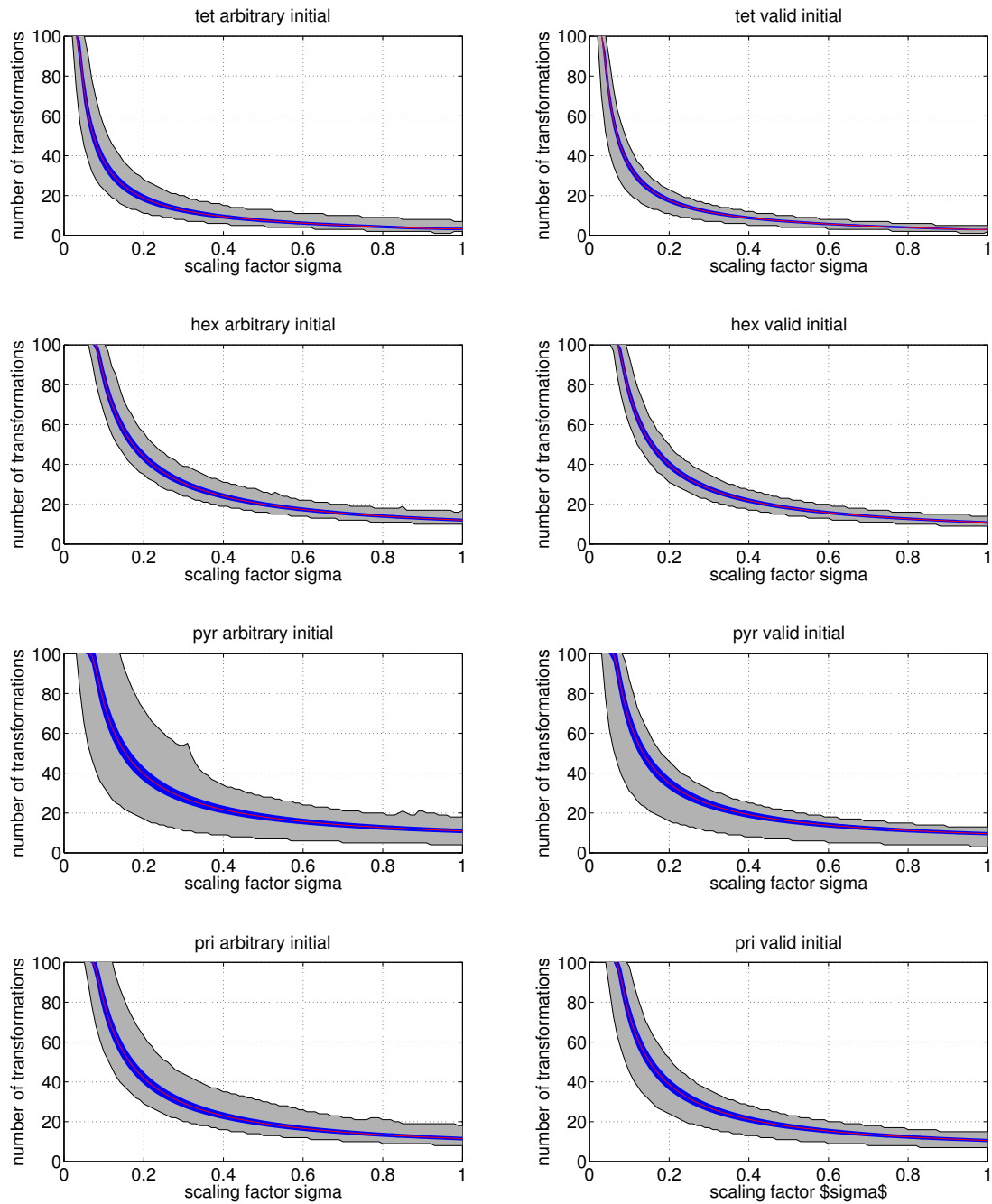


Fig. 7.2: Number of transformations depending on σ for tetrahedra, hexahedra, pyramids and prisms

Paper	Paper example			Dual element-based			$X^{\text{tet}}, X^{\text{hex}}, X^{\text{pri}}, X^{\text{pvr}}$ with $\sigma = 1$				
	Figure	q_{\min}^*	q_{mean}	Iter	CPU	q_{\min}^*	q_{mean}	Iter	CPU	q_{\min}^*	q_{mean}
[46]	Fig. 8	0.4177	0.7701	7/11700	0.2s	0.3918	0.7032	15/16100	0.2s	0.4413	0.7340
[46]	Fig. 11,12	0.2353	0.7433	9/2100	0.2s	0.0060	0.6100	15/2200	0.2s	0.0065	0.6891
[46]	Fig. 15 (S, U)	0.0293	0.7306	6/2100	1.3s	0.0141	0.7242	10/2200	1.8s	0.0246	0.7298
[46]	Fig. 15 (S, D)	0.0294	0.7300	10/2100	2.2s	0.0064	0.7109	17/2200	3.1s	0.0119	0.7206
[46]	Fig. 15 (M, U)	0.0174	0.7132	4/2100	3.0s	0.0162	0.7004	5/2400	3.1s	0.0046	0.7098
[46]	Fig. 15 (S, D)	0.0173	0.7105	10/2100	7.8s	0.0014	0.6644	16/2000	9.6s	0.0001	0.6923
[46]	Fig. 15 (L, U)	0.2680	0.7806	8/2100	6.2s	0.0120	0.7751	13/2100	8.5s	0.0044	0.7793
[46]	Fig. 15 (L, D)	0.2678	0.7805	11/2100	9.0s	0.0055	0.7685	17/2100	11.3s	0.0023	0.7760
[46]	Table 5, P	0.3942	0.7655	3/2100	0.0s	0.2537	0.7649	5/2100	0.0s	0.2516	0.7659
[46]	Table 5, TFire	0.5224	0.7861	5/2100	0.0s	0.4121	0.7868	8/2100	0.0s	0.4097	0.7873
[46]	Table 5, Cube1k	0.7655	0.8796	3/2100	0.0s	0.7190	0.8869	2/2200	0.0s	0.7190	0.8873
[46]	Table 5, House2	0.4010	0.7738	4/2100	0.0s	0.2877	0.7748	5/2100	0.0s	0.2868	0.7759
[46]	Table 5, Rand1	0.1999	0.4938	4/6500	0.2s	0.1441	0.4565	14/28100	0.5s	0.1932	0.4753
[46]	Table 5, Rire	0.3611	0.8110	8/2100	0.1s	0.1643	0.8111	12/2100	0.1s	0.1659	0.8122
[46]	Table 5, Cube10k	0.7087	0.8935	3/2100	0.0s	0.6288	0.8941	2/2200	0.0s	0.6287	0.8943
[46]	Table 5, Rand2	0.1022	0.4278	7/2100	0.4s	0.0043	0.3674	12/2100	0.5s	0.0019	0.3986
[46]	Table 5, Dragon	0.4886	0.9046	5/2000	0.2s	0.4190	0.9039	8/2000	0.3s	0.4180	0.9043
[46]	Table 5, Cow	0.4645	0.8470	9/2100	0.5s	0.4088	0.8447	13/2100	0.6s	0.4095	0.8455
[46]	Table 5, StGallen	0.5663	0.9004	4/2100	0.3s	0.3756	0.9002	7/2100	0.4s	0.3770	0.9007
[46]	Table 5, StayPuff	0.3347	0.8242	6/2100	1.0s	0.1576	0.8250	8/2100	1.2s	0.1563	0.8255
[43]	Fig. 5	0.0204	0.1199	12/2000	0.0s	0.0010	0.1090	19/2400	0.0s	0.0091	0.1164
[43]	Fig. 8	0.6619	0.8254	8/22900	0.5s	0.5199	0.8144	10/26500	0.6s	0.6210	0.8099
[43]	Fig. 12	0.4125	0.7235	17/10200	0.7s	0.4082	0.7146	26/22100	0.9s	0.3385	0.7207
[43]	Fig. 18	0.0052	0.7507	128/2000	687.0s	0.0043	0.7377	187/2400	726.7s	0.0029	0.7406
[43]	Fig. 19	0.0062	0.7492	118/2000	652.9s	0.0042	0.7220	179/2000	859.0s	0.0053	0.7370
[44]	Fig. 6	0.4476	0.8300	10/10000	1.0s	0.4277	0.8308	17/17300	1.5s	0.4537	0.8334
[44]	Fig. 10	0.2324	0.7437	13/4400	2.8s	0.1021	0.7274	27/2100	4.0s	0.10103	0.7420
[44]	Fig. 14	0.5522	0.8231	119/2100	30.5s	0.0638	0.8179	160/2100	32.9s	0.0939	0.8224
[45]	Fig. 10 tet	0.6591	0.8871	20/45800	33.7s	0.6591	0.8868	31/2700	30.2s	0.0023	0.8870
[45]	Fig. 10 hex	0.6125	0.9363	30/2100	4.9s	0.6125	0.9363	38/2200	5.1s	0.3459	0.9348
[41]	Fig. 5	0.3421	0.8637	12/2500	93.6s	0.3334	0.8638	19/7800	165.5s	0.3334	0.8643
[41]	Fig. 8	0.5442	0.9719	24/2100	238.5s	0.1335	0.9720	28/3200	162.5s	0.1498	0.9712

Table 7.2: Comparison with the dual element-based GETMe smoothing developed in [45]. First column: test cases with the results with the GETMe smoothing presented in the corresponding paper, second column: the results with the dual element-based method

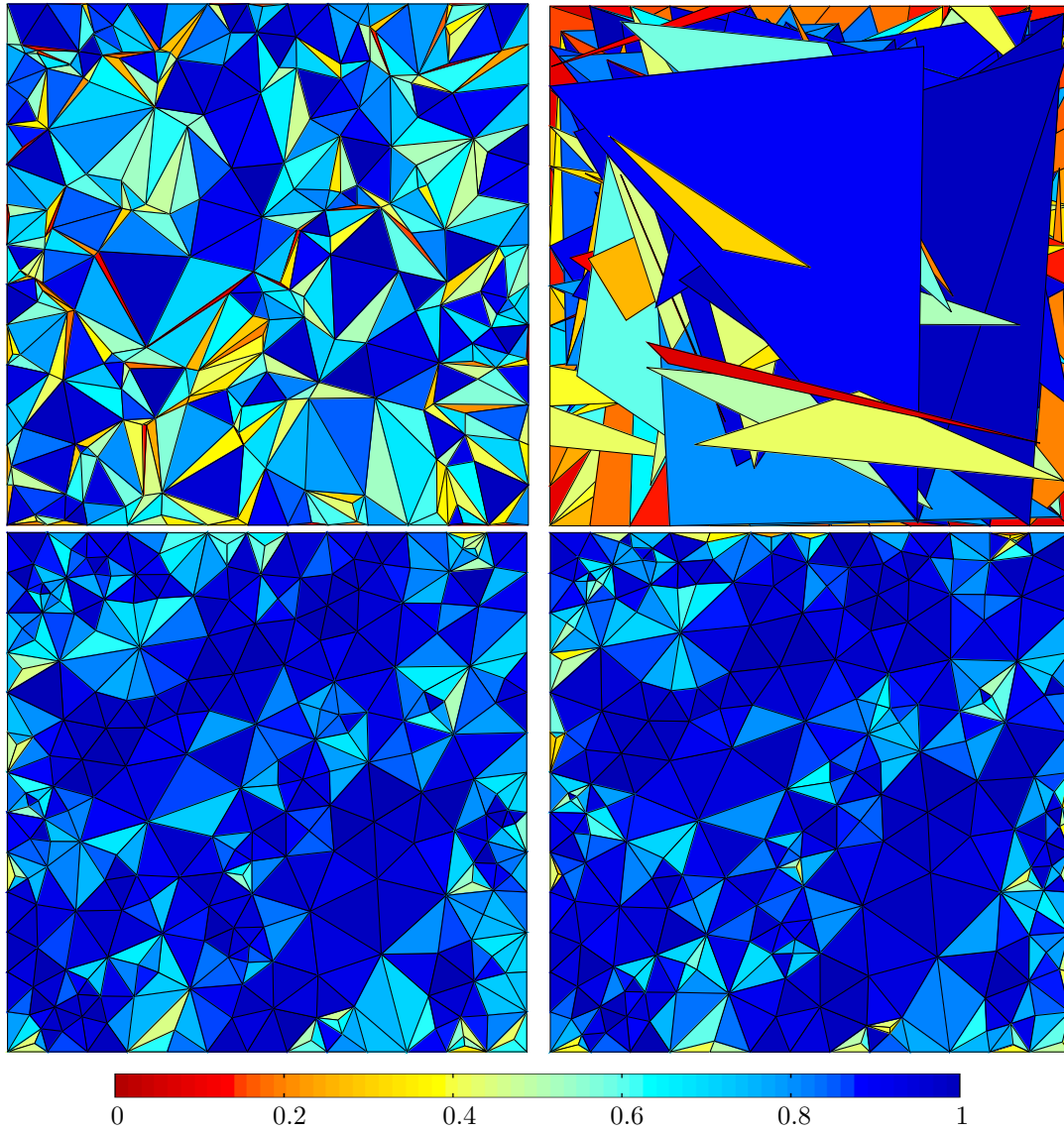


Fig. 8.1: The initial mesh (top left), a random mesh (top right) and the result optimizing $iq(E)$ (bottom left) for the initial mesh and the result optimizing $q(E)$ (bottom right) for a random mesh with each element colored according to its mean ratio quality number.